Kinetics and Catalysis, Vol. 43, No. 6, 2002, pp. 802–825. Translated from Kinetika i Kataliz, Vol. 43, No. 6, 2002, pp. 862–887.

Preparation, Structure, and Reactivity of ≡Si–N$^{\bullet}$–H Radicals

V. A. Radtzig

Semenov Institute of Chemical Physics, Russian Academy of Sciences, Moscow, 117977 Russia

Received June 11, 2002

Abstract—A method is developed for the synthesis of ≡Si–N$^{\bullet}$–H radicals on a silica surface and information is obtained by ESR and quantum chemical calculations of model systems on their structure and spectral (radiospectroscopic) characteristics. The reactivity of these radicals toward CO, H_2, and CH_2=CH_2 molecules is studied. The structure of the ≡Si–HN–C$^{\bullet}$=O radical is analyzed, which is the product of CO addition. The kinetic and thermochemical characteristics of processes with the participation of synthesized radicals are determined.

INTRODUCTION

Highly reactive species play an important role in various processes in the gas and condensed phases. Therefore, tremendous experimental and theoretical research effort is devoted to their structures and reactivity. To obtain these data, it is necessary to overcome substantial experimental difficulties. Therefore, the development of new methods for obtaining and stabilizing active species is promising. Point defects stabilized on the reactive silica surface [1, 2] possess high reactivity and can be used as a basis for constructing both paramagnetic and diamagnetic intermediates grafted on the surface. Gas phase molecules are the building blocks. This method proved to be very efficient for obtaining intermediates with various chemical compositions. Being bound via strong chemical bonds with the solid surface, these structures are thermally stable and do not have translational mobility. This fact together with the accessibility of these intermediates to the molecules of the surrounding medium open up unique possibilities for obtaining information on their spectral characteristics and reactivity toward various compounds. In [3], I reported the synthesis of various representatives of a series of hydrocarbon radicals. This work is devoted to the synthesis and study of the properties of nitrogen-centered free radicals. This paper reports on a method for synthesizing silicon-substituted nitrogen-centered radicals grafted to the SiO_2 surface and data on their spectral characteristics, structure, and reactivity. Reactions with the participation of radicals of this sort play an important role in atmospheric phenomena as well as hydrocarbon and in nitrogen-containing fuel combustion [4].

EXPERIMENTAL

In the experiments, the powders of high-dispersity Aerosil A-300 were used. Their specific surface area was ~300 m^2/g. The method of thermochemical activation of the silica surface resulting in a drastic increase in its chemical activity (the formation of so-called reactive silica (RSi)) was proposed by Morterra and Low and described in detail in [2, 5, 6]. It has been shown in [7] that this activity is associated with two types of defects on the surface of activated powder: (i) paramagnetic defects, which are $(\equiv Si–O)_3Si^{\bullet}$ radicals with a concentration of ~1×10^{12} cm^{-2} (or ~10^{17} per sample) and (ii) diamagnetic defects containing two-coordinated silicon atom $(\equiv Si–O)_2Si$: (>Si:). The concentration of the latter is higher by more than an order of magnitude [1, 2].

To obtain nitrogen-containing paramagnetic centers, NH_3 (ND_3) was used as a modifying molecule. All experiments were carried out under conditions of high vacuum or controlled atmosphere. The pressure of gases and vapors (N_2O, CO, NH_3, and others) in the system was measured using a Pirani gauge.

The registration of ESR spectra of the samples was carried out at 300 or 77 K using an EPR-20 spectrometer (Semenov Institute of Chemical Physics) working in the *X*-range.

Quantum chemical calculations were carried out using Gaussian 94 [8]. Fluorine-substituted molecular models of the defects of quartz with the ≡Si–O– groups replaced by fluorine atoms were used in calculations. For instance, the $F_2(HO)Si–N^{\bullet}–H$ radical modeled $(\equiv Si–O–)_2(HO)Si–N^{\bullet}–H$. As shown in [9], different types of paramagnetic and diamagnetic, intrinsic and impurity defects of silica and their fluorine-substituted low-molecular analogs have close physicochemical characteristics. One reason for this resemblance is the spatial localization of electronic states near the defect atom. Another reason is that the fluorine atom and the ≡Si–O– group have a similar substituent effect on the properties of the adjacent silicon atom.

0023-1584/02/4306-0802$27.00

The optimization of molecular structures was carried out using the gradient approximation of the density functional theory (DFT) in the variant of B3LYP/6–311G(*d*, *p*) or B3LYP/6–311G(2*d*, 2*p*) [10, 11]. For all optimized structures, we calculated their vibrational spectra. Each transition state (TS) had one negative eigenvalue of the Hessian matrix. The values of the reaction enthalpies at 0 K equal to $\Delta H(0\text{ K}) = \Delta E(0\text{ K}) + \Delta(ZPE)$ were calculated at the DFT level and in some cases at the G2MP2//B3LYP/6–311G(*d*, *p*) level. Here $\Delta E(0\text{ K})$ is the difference in the full energies of the initial reactants and products and $\Delta(ZPE)$ is the difference in the zero-point energies. In the case of G2MP2//B3LYP/6–311G(*d*, *p*), the calculation scheme of the G2MP2 method [12] was used but the optimization of the structure and the calculation of the vibrational spectra were carried by the B3LYP/6–311G(*d*, *p*) method. The G2MP2 method used to calculate the heats of formation of compounds usually provides better estimates of the thermochemical characteristics of a process than the DFT method. The calculation of energies (in atomic units) was carried out using the formula

$$E(\text{G2MP2(0 K)}) = E(\text{QCISD(T,E4T)/6–311G}(d, p)) + [E(\text{MP2/6–311 + G}(3df, 2p)) - E(\text{MP2/6–311G}(d, p))] + ZPE - 0.005n(\beta) - 0.0009(n(\alpha) - n(\beta)).$$

The first term in this expression is the energy of the structure at the QCISD(T,E4T)/6–311G(*d*, *p*) level [8]; the second term is a change in the system energy when the size of the basis set (the second bracket) is increased; the third term is the zero-point energy calculated at the DFT(B3LYP/6–311G(*d*, *p*)) level; and the other terms are the semiempirical higher-level correction [12], in which $n(\beta)$ is the number of β-electrons in the system and $(n(\alpha) - n(\beta))$ is the difference between the numbers of α- and β-electrons.

RESULTS AND DISCUSSION

1. Synthesis of Radicals (≡Si–O)$_2$(HO)Si–N•–H

To construct the radical of the mentioned type on the silica surface using the NH_3 molecule, two hydrogen atoms should be abstracted from an ammonia molecule and the residue with the silicon atom should be added to the SiO_2 surface. Radtsig and Kozlov [13] developed a method for obtaining the $>Si^{\bullet}–NH_2$ radicals on the silica surface. With this goal, we prepared the SiO_2 sample with the $(\equiv Si–O)_3Si–O^{\bullet}$ radicals and stabilized the diamagnetic centers of the silylene type >Si: on its surface. Oxy radicals were obtained by the thermal decomposition of their precursors, which are the $(\equiv Si–O)_3\equiv Si–N=N–O^{\bullet}$ radicals [14]: $\equiv Si–N=N–O^{\bullet} \longrightarrow \equiv Si–O^{\bullet} + N_2$. The amount of oxy radicals in the sample was measured by the volumetric method from the number of nitrogen molecules. It was $(1.2 \pm 0.1) \times 10^{16}$ radical/sample ($(2.4 \pm 0.2) \times 10^{17}$ g^{-1} or $(2.5 \pm 0.2) \times 10^{11}$ cm^{-2}).

Oxy radicals played the role of the generator of $^{\bullet}NH_2$ radicals by abstracting hydrogen atoms from ammonia molecules, whereas silylene centers efficiently accepted these species to form the paramagnetic centers $>Si^{\bullet}–NH_2$ (the concentration of acceptor groups was more than ten times higher than the concentration of paramagnetic centers):

$$\equiv Si–O^{\bullet} + NH_3 \longrightarrow \equiv Si–O–H + {}^{\bullet}NH_2, \quad \text{(I)}$$

$$>Si: + {}^{\bullet}NH_2 \longrightarrow >Si^{\bullet}–NH_2. \quad \text{(II)}$$

To obtain the nitrogen-centered free radical from this radical, it is necessary to abstract another hydrogen atom from nitrogen. We used the following procedure. Silyl radicals readily react with the nitrous oxide molecules [14]:

$$>Si^{\bullet}–NH_2 + N_2O \longrightarrow >Si(NNO^{\bullet})(NH_2). \quad \text{(III)}$$

Radicals formed are stable at room temperature but they readily decompose on heating above 373 K and eliminate a nitrogen molecule [14]. As this takes place, the oxy radical is formed. It could be assumed that the further transfer of the hydrogen atom from the amine group to this oxygen atom would result in the formation of the desired radical center:

$$>Si(NNO^{\bullet})(NH_2) \longrightarrow >Si(O^{\bullet})(NH_2) + N_2 \longrightarrow >Si(OH)(N^{\bullet}H). \quad \text{(IV)}$$

The last step of this process is exothermic: the strength of the O–H bond is ~10 kcal/mol higher than the strength of the N–H bond (see Section 3). A similar procedure has been used earlier for obtaining free radical centers [15]:

$$>Si^{\bullet}(C_2H_5) + N_2O \longrightarrow >Si(NNO^{\bullet})(C_2H_5)$$

$$\longrightarrow >Si(O^{\bullet})(C_2H_5) + N_2 \longrightarrow >Si(OH)(CH_2–CH_2^{\bullet}).$$

The complication in the realization of this program is that in the process of radical $>Si^{\bullet}–NH_2$ preparation a portion of ammonia molecules are adsorbed on the sample surface and that they cannot be removed even by long evacuation at 300 K. On the other hand, the $>Si^{\bullet}–NH_2$ radicals react with ammonia molecules even at room temperature, like all other silyl-type radicals [13]. In the presence of silylene centers on the sample surface, this leads to the formation of the $>Si^{\bullet}–H$ [13] radicals in the system:

$$>Si^{\bullet}–NH_2 + NH_3 \longrightarrow >Si(NH_2)_2 + H, \quad \text{(V)}$$

$$>Si: + H \longrightarrow >Si^{\bullet}–H. \quad \text{(VI)}$$

To prevent these reactions, the surface of reactive silica containing oxy radicals and silylene-type centers was treated with the mixture of gases NH_3 + N_2O with a composition 1 : 5 (at an overall pressure of ~0.1 Torr, 300 K) rather than with ammonia molecules. Under these conditions, ammonia molecules and nitrous oxide molecules do not enter chemical reactions with the silylene-type centers, and the nitrous oxide molecules are inert toward oxy radicals. The main reaction products are the $>Si(NNO^{\bullet})(NH_2)$ radicals. They are chemically inactive [14], and this fact makes it possible to prevent secondary reactions of the $>Si^{\bullet}–NH_2$ radicals with ammonia molecules.

Another advantage of this procedure was that the main portion of adsorbed ammonia molecules is removed when the sample containing $>Si(NNO^{\bullet})(NH_2)$ is heated to temperatures at which thermal decomposition (reaction (IV)) begins. However, we did not manage to exclude the secondary reactions with ammonia. After heating at 450 K (with the evacuation of the low-molecular products formed), we registered the $>Si^{\bullet}H$ and $>Si^{\bullet}–NH_2$ radicals in the sample in addition to the desired centers. Therefore, after heating to 450 K, the sample was allowed to stay at this temperature in an atmosphere of N_2O (10^{-2} Torr, 5 min). This made it possible to convert the main portion of the $>Si^{\bullet}–NH_2$ radicals formed in the course of this process into $>Si(OH)(N^{\bullet}H)$ (see reactions (III) and (IV)). In separate experiments after such treatment, the formation of the following radicals was detected in small amounts: $>Si(OH)(O^{\bullet})$ ($>Si^{\bullet}H + N_2O \longrightarrow >Si(NNO^{\bullet})(H) \longrightarrow >Si(O^{\bullet})(H) + N_2 \longrightarrow >Si^{\bullet}–OH + N_2O \longrightarrow >Si(NNO^{\bullet})(OH) \longrightarrow >Si(OH)(O^{\bullet}) + N_2$).

2. Radiospectroscopic Characteristics of the Radicals (≡Si–O)$_2$Si(OH)(N$^{\bullet}$H)

Figure 1 shows the ESR spectra of free radicals in the samples prepared according to the above procedure. The signal from the $(≡Si–O)_2\,{}^{28}Si(OH)({}^{14}N^{\bullet}H)$ radical (curve *1*) consists of four broad, slightly anisotropic components of the hyperfine structure. The position of the center of this signal corresponds to a value of the *g*-factor of 2.0045 ± 0.0005. The spectrum was recorded at 77 K. We failed to register the room-temperature ESR signal of the paramagnetic centers formed. This points to the considerable relaxational (reversible) broadening of the signal with an increase in temperature.

To assign the apparent constants of hyperfine interaction (HFI) to separate magnetic nuclei, we synthesized isotopically substituted radicals. Figure 1 (curve *2*) shows the ESR spectrum obtained using ND_3. The replacement of hydrogen by deuterium led to the transformation of the four-component signal into the three-component one and its narrowing by 20 G. Therefore, the value of the HFI constant of the unpaired electron and proton in the radicals is ~20 G. The principal triplet structure of this signal should be associated with the ^{14}N atom (I = 1, 100%). The value of the constant of HFI with a nitrogen nucleus is ~17 G. Moreover, we can notice additional splitting of the central component in the spectrum of the deuterated sample (curve *2*) into the three lines with distances between them of 3.1 ± 0.2 G. This should be associated with the presence of deuterium (I = 1).

Figure 1 (curve *3*) shows the ESR spectrum of the radical registered in the silica sample enriched in the ^{29}Si isotope (I = 1/2, the isotope concentration is 65%, whereas its natural concentration is 4.7%). Figure 1 shows the outermost components of the spectrum, which are a superposition of the signals from the paramagnetic centers involving the nuclei of the isotopes ^{28}Si (I = 0, 35%) and ^{29}Si (I = 1/2, 65%). The value of the constant of HFI with the ^{29}Si nucleus in this radical is 16 ± 2 G.

Thus, hydrogen, nitrogen, and silicon atoms are involved in the composition of the radical formed. Proceeding from the method of radical preparation, the observed ESR signal belongs to the $>Si(OH)(^{\bullet}NH)$ radical. We have not found data on the radiospectroscopic characteristics of the radicals of this sort in the literature. To interpret the experimental data, we used the results of quantum chemical calculation of the radiospectroscopic characteristics of the low-molecular models of the surface centers. To check the applicability of the computational schemes, we also calculated the radiospectroscopic characteristics of nitrogen-centered radicals of other types for which experimental data are available.

2.1. On the constant of HFI in nitrogen-centered radicals. Table 1 shows experimental data for the nitrogen-centered radicals $^{\bullet}NH_2$ [16], $^{\bullet}NF_2$ [17], and ≡Si–N$^{\bullet}$–Si≡ [18]. The latter was identified in the samples of nitrogen-doped sodium silicate glass. For the radical $^{\bullet}NH_2$, the isotropic values of the constant of HFI of an unpaired electron with nitrogen and protons were measured. An attempt to determine the anisotropic components of the corresponding tensors failed: the radical rotates in the argon matrix even at 8 K [16]. These data were obtained for the $^{\bullet}NF_2$ radical in the neon matrix [17] and for the ≡Si–N$^{\bullet}$–Si≡ radical [18]. Table 1 also shows the results of quantum chemical calculations of the radiospectroscopic characteristics of $^{\bullet}NH_2$, $^{\bullet}NF_2$, and $F_3Si–{}^{\bullet}N–SiF_3$ (models of the ≡Si–N$^{\bullet}$–Si≡ center) and $F_2(HO)Si–{}^{\bullet}NH$ and $F_3Si–{}^{\bullet}NH$ (models of $>Si(OH)(^{\bullet}NH)$).

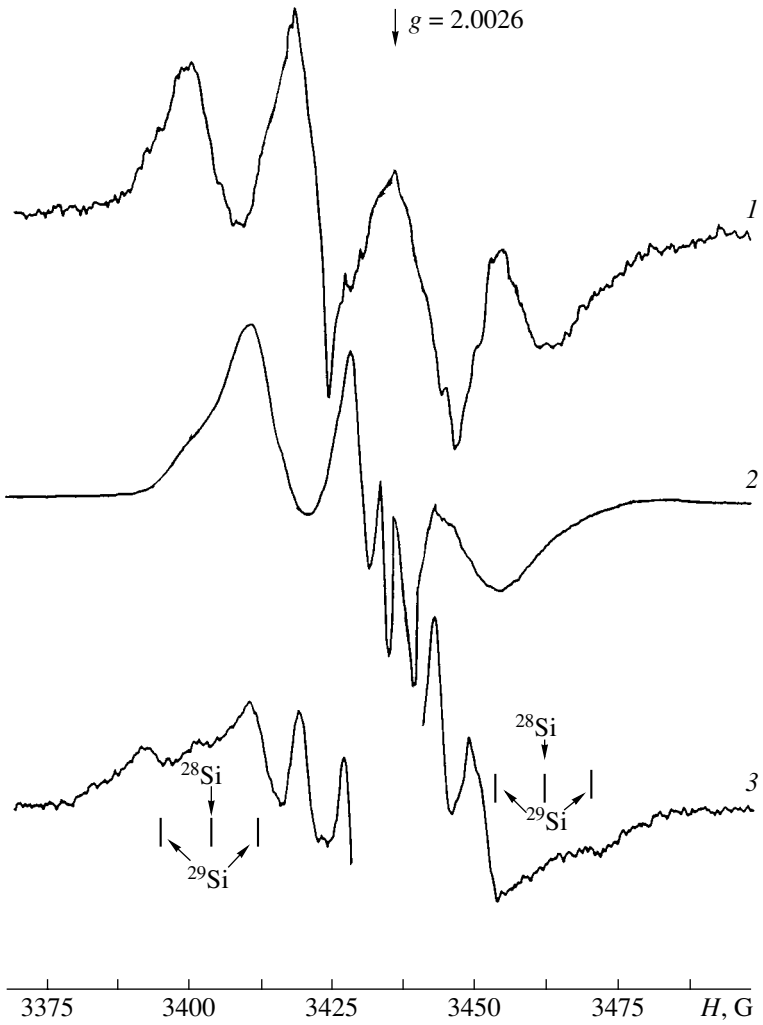

Fig. 1. ESR spectra of radicals $(\equiv Si–O)_2(HO)Si–\dot{N}H$ (77 K): (*1*) $(\equiv Si–O)_2(HO)^{28}Si–N\dot{H}$; (*2*) $(\equiv Si–O)_2(HO)^{28}Si–N\dot{}–D$; (*3*) $(\equiv Si–O)_2(HO)^{28}Si–\dot{N}–H$ (35%) + $(\equiv Si–O)_2(HO)^{29}Si–\dot{N}–H$ (65%).

Figure 2 shows the optimized structures of the radicals $F_3Si–\dot{N}–SiF_3$, $F_2(HO)Si–\dot{N}H$, and $F_3Si–\dot{N}H$. The optimization of the geometry of the first radical was carried out using the DFT calculation and at the UB3LYP/6–311G(2*d*,2*p*) level. The use of the extended basis set makes it possible to obtain a more exact estimate of the valence angle Si–N–Si in the radical. A similar situation appears in the optimization of structures involving the siloxane bridge Si–O–Si. For the $F_3Si–O–SiF_3$ molecule, the optimized values of the valence angle Si–O–Si was 167.2° and 145.2° as calculated by the B3LYP/6–311G(*d, p*) and B3LYP/6–311G(2*d*,2*p*) methods, respectively, whereas the experimental value is 155.7° [19].

Comparison of calculated and experimental data for the radicals $\dot{N}H_2$, $\dot{N}F_2$, and ≡Si–N˙–Si≡ suggests that calculations underestimate the isotropic constants of HFI with the nitrogen nucleus and proton but rather accurately estimate the anisotropic components of the corresponding tensors. Note that, in the $X_3Si–\dot{N}H$ radicals, the isotropic and anisotropic components of tensors of HFI of an unpaired electron with the nitrogen nucleus and proton have comparable values. For the ^{29}Si nucleus, the main contribution is from isotropic HFI.

2.2. On the *g*-tensor of nitrogen-centered radicals. In the ground electronic state of nitrogen-centered radicals, an unpaired electron is localized on the $2p_x$-AO nitrogen, whose symmetry axis is perpendicular to the plane of atoms Y–N–X. The first electronically excited state in radicals of this type is due to electron transfer from the unshared electron pair of nitrogen onto the orbital partially occupied by an unpaired electron [18]. When the electronegativity of substituents at the nitrogen atom decreases, the difference in the energies of these states decreases. According to experimental data, this difference is ~5 eV for the radical $F–\dot{N}–F$ [20] and

Table 1. Experimental (exptl) and calculated (clcd) (UB3LYP/6–311G(*d*, *p*)) values of radiospectroscopic characteristics (G) of nitrogen-centered radicals

Radical	a_{iso} (^{14}N)	b_1	b_2	b_3	a_{iso} (^{1}H)	b_1	b_2	b_3	a_{iso} (^{29}Si)	b_1	b_2	b_3
$^{\bullet}NH_2$ (exptl) [16]	10.5	–	–	–	|24.0|	–	–	–	–	–	–	–
$^{\bullet}NH_2$ (clcd)	7.4	31.4	–15.4	–16.0	–22.0	–3.8	7.2	–3.6	–	–	–	–
$^{\bullet}NF_2$ (exptl) [17]	16.3 ± 1	32.6	–16.3	–16.3	–	–	–	–	–	–	–	–
$^{\bullet}NF_2$ (clcd)	12.2	33.7	–16.4	–17.3	–	–	–	–	–	–	–	–
$F_3Si–^{\bullet}NH$ (clcd)	7.2	29.0	–14.5	–14.5	–18.8	22.0	–18.0	–4.0	–17.3	1.0	0.4	–1.4
$F_2(HO)Si–^{\bullet}NH$ (clcd)	7.7	28.9	–14.5	–14.4	–20.4	21.9	–18.4	–3.4	–16.4	0.6	0.1	–0.7
≡Si–$N^{\bullet}$–Si≡ (exptl) [18]	12–13	23–24	–12	–12	–	–	–	–	–	–	–	–
$F_3Si–N^{\bullet}–SiF_3$ (clcd)	7.2	27.3	–13.5	–13.8	–	–	–	–	–14.5	0.7	0.2	–0.9

~2 eV for the radical H–$^{\bullet}$N–H – [21]. DFT calculations (UB3LYP/6–311G(*d*, *p*)) provided estimates of the energies of these vertical transitions: 4.49 and 2.14 eV, respectively. These values agree with the experimental data obtained in this work.

For the radicals ≡Si–$N^{\bullet}$–H and ≡Si–$N^{\bullet}$–Si≡, experimental data on the energies of these transitions are not available. Calculations suggest their further decrease to 1.02 and 0.48 eV in the radicals $F_3Si–^{\bullet}NH$ and $F_3Si–^{\bullet}N–SiF_3$, respectively. In the case of the latter radical, this effect is partially due to an increase in the value of the valence angle Si–N–Si (136.3°). To remind, as the valence angle in the radicals X–$^{\bullet}$N–Y approaches 180°, the energies of the ground state and the excited state under consideration in radicals of this type become closer. When the angle is 180°, the electronic state of the radical becomes degenerate. According to the results of calculations of nitrogen-centered radicals that have hydrogen or silicon atoms as substituents at the nitrogen atom, other excited states are much higher (~5 eV).

The existence of the low electronically excited state leads to the deviation of one of the components (g_z) of the *g*-tensor of the radical Y–$^{\bullet}$N–X (the *z* axis is in the plane of the radical and its direction is close to the perpendicular of the bisecting line of the valence angle Y–N–X (the *y* axis)) from the value $g_e = 2.0023$, which is characteristic of a free electron. The value of the shift can be estimated using the formula [22]

$$\Delta g_z = g_z - g_e \cong 2\lambda c_1^2 c_2^2 / \Delta E, \quad (1)$$

where $\lambda = 76$ cm^{-1} is the constant of spin–orbital interaction for the nitrogen atom [23], c_1^2 and c_2^2 are the populations of the $2p_x$- and $2p_y$-AO of nitrogen in the ground and electronically excited states, and ΔE is the difference in the energies of these states. Here we used the two-level approximation, because other excited states of the radicals are noticeably higher in radicals of the considered type.

Let us estimate the value of the shift of the corresponding component of the *g*-tensor of the radical H–$^{\bullet}$N–H. Upon substituting the calculated values $c_1^2 = 0.98$, $c_2^2 = 0.72$, and $\Delta E = 2.14$ eV into formula (1), we obtain $\Delta g_z \cong 0.00625$. If we assume that two other components of the *g*-tensor are close to the values corresponding to a free electron, then we obtain a g_{iso} value of 1/3(2.0023 + 2.0023 + 2.0086) = 2.0044. This is lower than the experimental value (2.0058 [16]), but it is necessary to take into account several assumptions made for obtaining estimates.

Analysis of the form of the ESR spectrum of the radicals ≡Si–$N^{\bullet}$–Si≡ in sodium silicate glass led Mackey *et al*. [18] to the conclusion that the separate groups of radicals differ in the values of one of the principal component of the *g*-tensor (from 2.008 to 2.024 for the component g_z according to the notation used in [18]). Figure 3 shows the function of distribution of the number of radicals borrowed from [18]. They are characterized by a certain value of g_z, using which Mackey *et al*. managed to reproduce the form of the experimental ESR signal.

The values of g_z for separate groups of radicals are largely determined by the value of ΔE (formula (I)), which in turn depends on the value of the valence angle Si–$N^{\bullet}$–Si. According to [18], the value of this angle differs for different groups of radicals and is determined by the (disordered) structure of the solid. The corresponding dependence can be calculated using quantum chemical methods. The radical ≡Si–$N^{\bullet}$–Si≡ was used to model the paramagnetic center $F_3Si–^{\bullet}N–SiF_3$.

The optimized geometry of the radical has C_2 symmetry. This made it possible to calculate the energies of two lower electronic states of the radical (^2B and ^2A) corresponding to two irreducible representations of this symmetry group. These are the ground (^2B) and the first electronically excited (^2A) states. Figure 3 shows the dependences of electron energy on the value of the valence angle Si–N–Si in the radical electron energy, the value of ΔE (the energy of the first excited state (vertical $^2B \longrightarrow {}^2A$ transition)), and the values of the component g_z calculated using formula (1). Noticeable changes in the energies of these structures appear with a decrease in the value of the valence angle to 110°. At the same time, a change in the valence angle Si–N–Si in the range 110°–180° leads to the differences in the energies of radical transition to the first electronically excited state. Thus, according to calculations, the values of the g_z-component ranging from 2.008 to 2.024 correspond to the values of the valence angle Si–N–Si ranging from 110° to 130° and the energies of the first excited state $1.2 \geq \Delta E \geq 0.5$ eV. This estimate seems to be realistic. The calculations show that the nitrogen atom in the compounds $N(SiH_3)_3$ and $N(SiF_3)_3$ are in the planar coordination. Probably this is also true of the fragment $N(Si\equiv)_3$ in quartz, and then the angle Si–N–Si in it is close to 120°, whereas for the optimized structure of the radical $F_3Si–N^{\bullet}–SiF_3$, the angle Si–N–Si is 136.3°.

Based on the above analysis, we draw the following conclusions on the expected radiospectroscopic characteristics of nitrogen-centered radicals: (1) the tensor of HFI of an unpaired electron with the nitrogen nucleus has axial symmetry with the parallel component equal to 36–42 G and the perpendicular component close to zero ($a_{iso}(^{14}N)$ =12–16 G); (2) radicals in which hydrogen and silicon atoms are the substituents at the nitrogen atom have a low electronically excited state with which the shift of one of the components of the *g*-tensor is associated.

2.3. Modeling the ESR spectrum of the radical ≡Si–N˙–H. There is no reason to expect the distribution over valence angles Si–N–H for the radical ≡Si–N˙–H stabilized in the silica surface. The calculated equilibrium value of the valence angle Si–N–H for its low-molecular model (the radical $F_3Si–N^{\bullet}–H$) is 114.6°, and the value of the energy of vertical transition to the electronically excited state ΔE is 1.02 eV. By substituting the calculated values for the radical $F_3Si–{}^{\bullet}N–H$ into formula (1) ($c_1^2 = 0.92$, $c_2^2 = 0.72$, and ΔE =1.02 eV), we obtain that $\Delta g_z \cong 0.0138$. That is, there is a noticeable shift of one of the components of the *g*-tensor of the radical. In this case, the value of g_{iso} is ~2.007 (assuming that two other principal components of the *ART*-tensor are 2.0023). We should also expect the anisotropy of the constants of HFI of an unpaired electron with the nitrogen nucleus and proton in this radical (see Table 1). However, we cannot find this specific feature in the ESR spectra shown in Fig. 1.

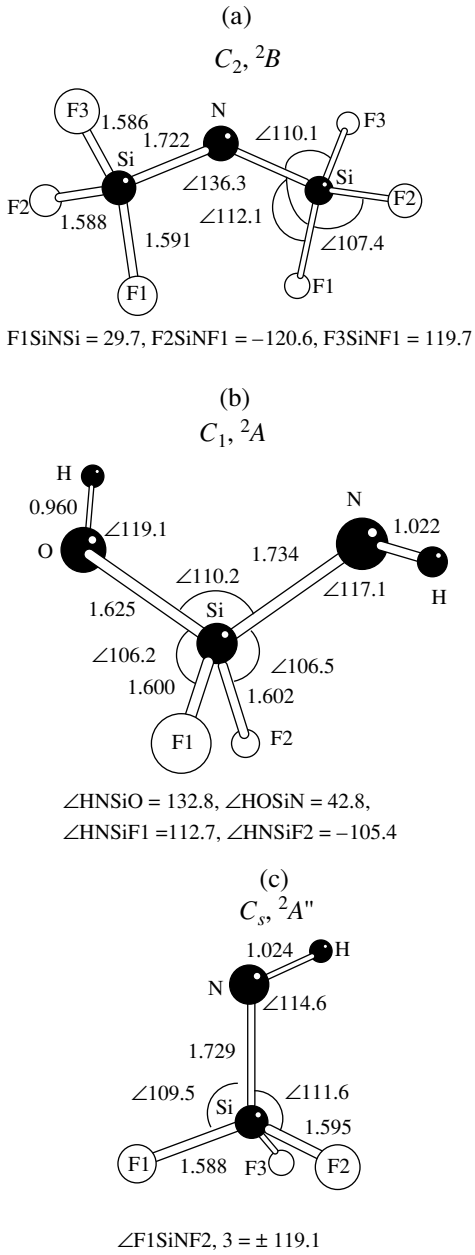

Fig. 2. Optimized structures of nitrogen centered radicals (UB3LYP/6–311G(2*d*, 2*p*)): (a) $F_3Si–{}^{\bullet}N–SiF_3$ (6-311G(2*d*, 2*p*) basis set); (b) $F_2(HO)Si–{}^{\bullet}N–H$; and (c) $F_3Si–{}^{\bullet}N–H$. Bond lengths are in Å; the angles are in degrees.

In our opinion, the reason is that the rotation of the N–H group around the Si–N bond in this radical is possible at a temperature as low as 77 K. Figure 4 shows the results of calculating the profile of the potential energy surface for the rotation of the N–H group around

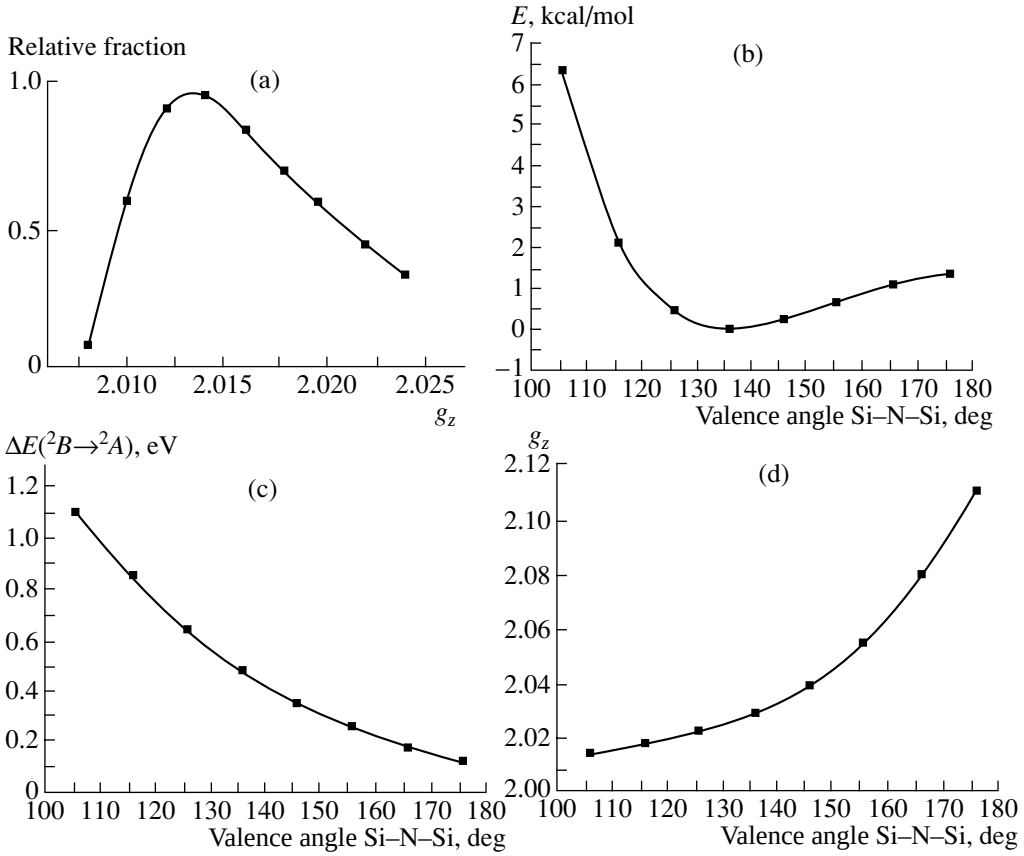

Fig. 3. Radiospectroscopic characteristics of radicals ≡Si–$^{\bullet}$N–Si≡: (a) relative fraction of radicals ≡Si–$^{\bullet}$N–Si≡ on sodium silicate glass characterized by a certain value of one of the principal components of the *g*-tensor (according to [18]); the dependences of (b) electronic energy, (c) the energies of the first excited state (the energy of the vertical transition $^2B \longrightarrow {}^2A$), and (d) the values of g_z (calculation using Eq. (1)) for the radical $F_3Si–{}^{\bullet}N–SiF_3$ (spatial symmetry group C_2) on the value of the valence angle Si–N–Si (DFT calculations UB3LYP/6–311G(2*d*, 2*p*)).

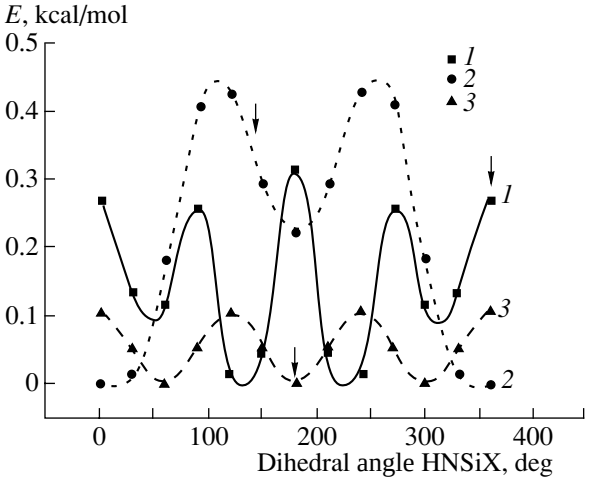

Fig. 4. Potential energy surface profiles for the rotation of the N–H group around the Si–N bond in the radicals ≡Si–$^{\bullet}$N–H (DFT calculations UB3LYP/6–311G(*d*, *p*)): (*1*) F_2(HO)Si–$^{\bullet}$N–H, (*2*) F_2(HO)Si–$^{\bullet}$N–H at a fixed position of the OH group, and (*3*) F_3Si–$^{\bullet}$N–H.

the Si–N bond in the radical F_2(HO)Si–$^{\bullet}$NH. In the calculations, we fixed the value of the dihedral angle HNSiO and optimized all other geometric parameters, including the orientation of the OH group (the value of the dihedral angle NSiOH) (Fig. 4, curve *1*). In this model, the rotation of the NH group is accompanied by the rotation of the OH because, for the *trans*-configuration of atoms H, N, Si, and O, the *cis* position of H, O, Si, and N atoms is energetically preferable and vice versa. In another model, the rotation of the NH group takes place when the spatial arrangement of the OH group in the radical is frozen (the angle HOSiN was taken as equal to 180°) (Fig. 4, curve *2*). Thus, freezing the OH group leads to a noticeable change in the potential energy surface profile for the rotation of the NH group in the radical. Finally, the same figure (curve *3*) shows the results of calculating the profile of the potential energy surface for the rotation of the NH group in the radical $F_3Si(^{\bullet}NH)$. A change in the structure of the coordination sphere of the silicon atom (an increase in its symmetry) resulted in a noticeable change in the

height of the activation barrier. Note that an increase in the mobility of free-radical fragments –O–$CH_2^•$ and –N=N–O• bound to the silicon atom with a change in the structure of its coordination sphere ($(\equiv Si–O)_2(HO)Si \longrightarrow (\equiv Si–O)_3Si$) has been experimentally detected [14].

Thus, the calculation shows that the height of the potential barrier E to the internal rotation of the NH group in the radical $((\equiv Si–O)_2(HO)Si–^•NH$ is at most 0.5 kcal/mol. This means that the frequency of rotation of this group at 77 K ($\approx 10^{12}\exp(-E/RT)$ s^{-1}) is higher than 10^{10} s^{-1}. Rotation with frequencies higher than 10^8 s^{-1} leads to the averaging of the anisotropic components of the g-tensor and the tensor of HFI of an unpaired electron with the magnetic nuclei ^{14}N and ^1H in the radical. This averaging is only partial because rotation is monoaxial. Therefore, we assume that, even at 77 K, the ESR spectrum of the radical $(\equiv Si–O)_2(HO)Si–^•NH$ corresponds to the case of fast monoaxial rotation of the NH group around the Si–N bond, and its form is determined by the averaged values of the components of g- and a-tensors (which are axially symmetric in the first approximation). Lines corresponding to the perpendicular components of these tensors have the highest intensities in the spectrum. Then, the radiospectroscopic characteristics of the radical determined from the spectra in Fig. 1, which are $g = 2.0045 \pm 0.0005$, $a(^{14}N) = 17 \pm 1$ G, $a(^1H) = 20 \pm 1$ G, and $a(^{29}Si) = 16 \pm 2$ G, should be assigned to the perpendicular components of the corresponding tensors.

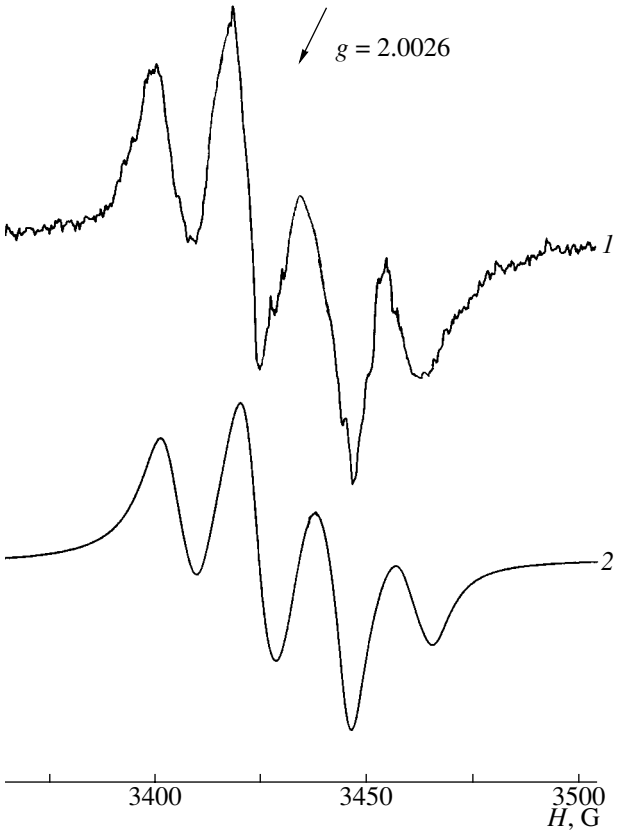

Fig. 5. (*1*) Experimental and (*2*) simulated spectra of the ESR radical $^{28}Si–N^•–H$ (the spin-Hamiltonian parameters are given in the text).

Using the results of quantum chemical calculation for the model of monoaxial rotation of the NH group in the radical, we can estimate its expected radiospectroscopic characteristics. The direction of the z axis is at an angle of 32.5° to the rotation axis (see Fig. 2). If we assume that $g_x \cong g_y \cong 2.0023$, $g_z \cong 2.0023 + 0.0138 = 2.016$ ($g_{iso} = 2.0069$), then we obtain for this model: $g_\parallel = [g_z^2\cos^2(32.5) + g_y^2\sin^2(32.5)]^{1/2} = 2.012$, $g_\perp = 1/2(3g_{iso} - g_\parallel) = 2.0043$, $a_\parallel(^{14}N) \cong 0$, $a_\perp(^{14}N) \cong 18$ G, $a_\parallel(^1H) \cong -17$ G, and $a_\perp(^1H) \cong -21.5$ G (the tensor of HFI of an unpaired electron with the nucleus of the nitrogen atom was chosen in the form $a_x = 36$ G, and $a_y = a_z = 0$ and that with a proton was $a_x = -2$, $a_{y'} = -32$, and $a_{z'} = -18$ G; the y' axis is directed along the N–H bond; see Table 1). According to calculation, isotropic (contact) interaction contributes most greatly to the constant of HFI of an unpaired electron with the ^{29}Si nucleus in the radical. The anisotropic components of the corresponding tensor are small (see Table 1). The value of this splitting is ~15 G in agreement with the experimentally determined value 16 ± 2 G (see above). Thus, there is acceptable agreement between the observed radiospectroscopic constants and those calculated within the framework of this model for the radical ≡Si–N• –H.

Figure 5 shows the ESR spectrum of the radical $\equiv^{28}Si–^{14}N^•–^1H$ calculated for the polycrystalline sample with the axially symmetric spin Hamiltonian

$$H = g_\parallel \beta \vec{H}_0 \hat{\vec{S}} + g_\perp \beta \vec{H}_0 \hat{\vec{S}} + \hat{\vec{S}}\hat{a}(^{14}N)\hat{\vec{I}}(^{14}N) + \hat{\vec{S}}\hat{a}(^1H)\hat{\vec{I}}(^1H)$$

and the following principal values of the g- and $\hat{a}$-tensors: $g_\parallel = 2.012$, $g_\perp = 2.0043$, $a_\parallel(^{14}N) = 2$ G, $a_\perp(^{14}N) = 17$ G, $a_\parallel(^1H) = -20$ G, and $a_\perp(^1H) = -20$ G; $\vec{H}_0$ is the magnetic field, β is the Bohr magneton for an electron, $\hat{\vec{S}}$ is the electron spin, and $\hat{\vec{I}}$ is the nucleus spin. The values of the perpendicular components of tensors were taken from the experimentally observed ESR signals (Fig. 1), and the values of the parallel components were calculated. In the simulation of the spectrum, we used the Lorentz form of individual lines. It was taken differently for the parallel and perpendicular orientation of

Fig. 6. ESR spectra of the products of radical ≡Si–$^{\bullet}$N–H reactions with CO (registered at 77 K): (*1*) the product of interaction of the radical ^{28}Si–$^{\bullet}$N–H with CO at 77 K (radical **A**); (*2*) the result of simulation of spectrum *1* (see text); (*3*) the product of interaction of the radical ≡^{29}Si–$^{\bullet}$N–H with CO at 77 K; (*4*) after heating the product characterized by spectrum *1* to 300 K, radical **B** (arrows show two lines belonging to radicals **A**); (*5*) radical **B** in the sample enriched in the ^{29}Si isotope (the positions of lines of radicals **B** containing various silicon isotopes are schematically shown).

the radical (6 and 4 G, respectively). The additional broadening of the parallel component made it possible to achieve better agreement between experimental and calculated ESR spectra. Note that the position of separate HFI constants of the ESR spectrum in this case is largely determined by the values of the perpendicular components of the *g*- and *a*-tensors.

Other evidence for the structure ≡Si–N$^{\bullet}$–H of paramagnetic centers formed was obtained in the study of their reactivity. Below we discuss the results of the study of processes with the participation of radicals ≡Si–N$^{\bullet}$–H and molecules CO, H_2, and C_2H_4.

3. Reaction ≡*Si–N*$^{\bullet}$*–H + CO* ⟶ ≡*Si–HN–C*$^{\bullet}$*=O*

Radicals ≡Si–N$^{\bullet}$–H and ≡Si–O$^{\bullet}$ are isoelectronic, and this fact assumes that there is some similarity in their properties. Due to the specific features of the electronic structures of radicals ≡Si–O$^{\bullet}$ (the electronic state is close to the degenerate one), their registration by the ESR method is difficult [1, 2]. A convenient method for detecting these radicals is the use of CO molecules, which can undergo addition to these radicals at a temperature as low as 77 K to form the paramagnetic centers ≡Si–O–C$^{\bullet}$=O [24]. One might expect that radicals ≡Si–N$^{\bullet}$–H would also react with the CO molecules to

form the acyl-type centers ≡Si–HN–C•=O. Below we provide the results of this study.

The interaction of the sample containing radicals ≡Si–N•–H with the molecules ^{12}CO (at 77 K and $P_{CO} \approx 10^{-2}$ Torr) was accompanied by the formation of new paramagnetic centers. The process was monitored by the ESR method. Figure 6 (curve *1*) shows the ESR spectrum of the reaction product $(\equiv Si–O)_2(HO)$ $^{28}Si–HN–C^{\bullet}=O$ (radical **A**). It consists of four anisotropic components of the hyperfine structure and has the following radiospectroscopic characteristics: $g_1 = 1.9983 \pm 0.0002$, $g_2 = 2.0028 \pm 0.0002$, $g_3 = 2.0043 \pm 0.0002$, $g_{iso} = 2.0018 \pm 0.0002$; $a_1(^{14}N) = 29.0 \pm 0.5$ G, $a_2(^{14}N) = 30.4 \pm 0.5$ G, $a_3(^{14}N) = 27.8 \pm 0.5$ G, $a_{iso}(^{14}N) = 29.1 \pm 0.5$ G; and $a_1(^1H) = 32.0 \pm 0.2$ G, $a_2(^1H) = 30.4 \pm 0.5$ G, $a_3(^1H) = 27.8 \pm 0.5$ G, and $a_{iso}(^1H) = 30.1 \pm 0.5$ G (these values were determined assuming that the principal axes of all tensors coincide).[1] For comparison, we provide the *g*-tensor of the isoelectronic radical $(\equiv Si–O)_2(HO)Si–O–C^{\bullet}=O$ (77 K): $g_1 = 1.9977 \pm 0.0002$, $g_2 = 2.0012 \pm 0.0002$, $g_3 = 2.0031 \pm 0.0002$, and $g_{iso} = 2.0007 \pm 0.0002$ [25]. The result of simulating the ESR spectrum of radical **A** with the above-mentioned parameters of the spin Hamiltonian (in the second-order perturbation theory and the Gaussian form of the individual component with a half-width of 0.5 G) is shown in Fig. 6 (curve *2*).

When a silica sample is enriched in the ^{29}Si isotope (65%), the ESR spectrum of the product has a similar form (Fig. 6, curve *3*). The difference is that some hyperfine structure components are wider. This points to the fact that the constant of HFI of an unpaired electron with the ^{29}Si nucleus in this radical is ~3 G (as estimated from the apparent broadening of lines in this spectrum).

Sample heating to 300 K results in irreversible change in the form of the ESR spectrum, but their concentration does not change (within a limit of 20%). The transformation occurs in the temperature range 160–190 K. The ESR spectra of reaction products in the ordinary silica sample and the sample enriched in the ^{29}Si isotope are shown in Fig. 6 (curves *4*, *5*) (77 K) and Fig. 7 (300 K). The ESR spectrum of the newly formed radical **B** (Fig. 7, curve *1*) at 300 K is characterized by $g_{iso} = 2.0020 \pm 0.0002$ and consists of three slightly asymmetric hyperfine structure components with an intensity ratio of 1 : 1 : 1 and a splitting between them of 20.9 ± 0.5 G. The apparent hyperfine structure is due to the interaction of an unpaired electron with the ^{14}N nucleus ($I = 1$). The asymmetry of the HFI components points to small anisotropy of the *g*-tensor and the tensor of HFI of an unpaired electron with the nitrogen nucleus in the radical.

For the silica sample enriched in ^{29}Si isotopes (65%), the ESR spectrum of radical **B** contains the additional doublet splitting (32 G) of each of the three components of the hyperfine structure (curve *5* in Fig. 6 and curve *2* in Fig. 7). This is due to the interaction of an unpaired electron with the nucleus ^{29}Si ($I = 1/2$). In this case the observed signal is the superposition of the spectra of radicals containing silica isotopes ^{29}Si (65%) and ^{28}Si (35%).

A small extrinsic component (~5%) from the ESR signal of the initial radical is distinguishable on the wings of the ESR spectrum shown in Fig. 6 (curve *4*). The lines corresponding to the initial radical are marked with arrows. When the spectrum was registered at 300 K, the ratio of intensities of the ESR signals from radicals **B** and **A** was $(0.80 \pm 0.05) : (0.20 \pm 0.05)$ (Fig. 7). Thus, two radical centers are in equilibrium with each other, and the equilibrium constant at room temperature is 0.25 ± 0.07. Below, we provide evidence for the fact that radicals **A** and **B** have the structure $(\equiv Si–O)_2(HO)Si–HN–C^{\bullet}=O$ but differ in the spatial arrangement of their atoms in the fragment Si–N–C=O (*trans* for radical **A** and *cis* for radical **B**). Since the fraction of radicals **A** in the ESR spectrum decreases when the sample is cooled to 77 K, the *cis* configuration of the radical is characterized by the lower enthalpy of formation. The form of the ESR signals of radicals **A** and **B** (Figs. 6 and 7) reversibly depend on the registration temperature but these changes are insignificant.

An analogous ESR signal appears if the reaction with CO is carried out at room temperature. Under these conditions, the concentration of radicals in the sample can be determined by the volumetric method from the amount of chemisorbed CO molecules.[2] According to the results of measurements, their amount in the sample was $(1.0 \pm 0.1) \times 10^{16}$. For comparison, the amount of radicals ≡Si–O• in the sample used for the preparation of nitrogen-centered radicals was $(1.2 \pm 0.1) \times 10^{16}$ (see Section 2). Thus, multistage preparation of nitrogen-centered radicals (see Section 1) only leads to an insignificant decrease in the concentration of radicals in the sample.

Data on the constants of HFI of an unpaired electron with the nucleus ^{13}C in radicals **A** and **B** were obtained in the experiments with CO enriched in the

[1] In the radical $(\equiv Si–O)_2(HO)Si–HN–C^{\bullet}=O$, the symmetry of the silicon atom environment is $(Si(OH)(O–Si\equiv)_2)$. Therefore, the highest possible symmetry of the potential field in which the NHCO group rotates around the Si–N bond is C_s, and even fast rotation in such a potential should not necessarily lead to the axial symmetry of the corresponding tensors. Hence, the fact that the ESR spectrum of radical **A** at 77 K is characterized by three principal values of the *g*- and HFI-tensors does not necessarily point to the existence of the radical in the frozen equilibrium conformation.

[2] At 77 K, these measurements are difficult to carry out because of the adsorption of a large portion of CO molecules on the high-dispersity silica surface (which greatly exceed the quantity of radicals).

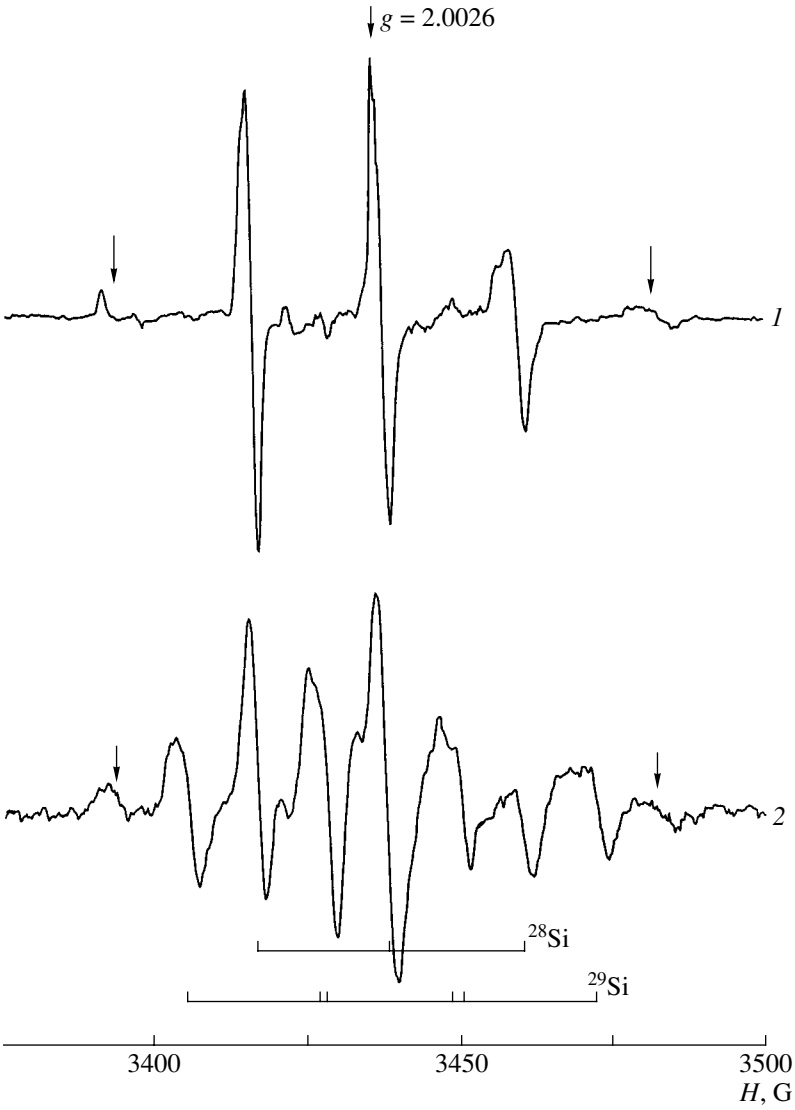

Fig. 7. ESR spectra of radicals ≡Si–NH–C$^{\bullet}$=O on the surface of (*1*) conventional silica and (*2*) silica enriched in the ^{29}Si (65%) isotope. The spectra were registered at 300 K. The arrows mark two lines that refer to the acyl radicals of type **A** (see text).

^{13}C isotope (85%). The nitrogen-centered radicals were $(\equiv Si{-}O)_2(DO)Si{-}N^{\bullet}{-}D$. The preparation of these radicals was carried out using ammonia ND_3. The use of deuterium-containing radicals simplified the interpretation of the experimental data: in this case the ESR spectra of radicals containing ^{12}C and ^{13}C isotopes do not overlap.

The reaction with the CO molecules was carried out at 77 K. The observed ESR signal is the superposition of two signals from radicals involving isotopes ^{13}C and ^{12}C. A portion of the ESR spectrum that is due to radicals containing ^{12}C is a triplet with 30-G splitting due to the interaction of an unpaired electron with the nucleus ^{14}N. Each component of the triplet further splits because of the interaction of an unpaired electron with the nucleus D (I = 1). In the hydrogen-containing radical of this type the value of the constant of HFI with proton is ~30 G (see above), and it is ~4.5 G in the deuterium-containing radical (in proportion to the magnetic momentums of proton and deuteron, equal to 6.51).

The ESR spectrum of the radical containing ^{13}C is shown in Fig. 8 (curve *1*). This is a doublet (due to ^{13}C ($I = 1/2$)) of triplets (due to ^{14}N ($I = 1$), and $a(N) \approx 30$ G). Besides that, a poorly resolved hyperfine structure is observed, which is due to the interaction of an unpaired electron with the nucleus D ($a(D) = 4.5 \pm 0.25$ G). Assuming that the tensor of HFI of an unpaired electron with the nucleus ^{13}C has axial symmetry, we obtain $a_{\parallel}(^{13}C) = (188 \pm 2)$ G and $a_{\perp}(^{13}C) = (158 \pm 1)$ G ($a_{iso}(^{13}C) = 168 \pm 2$ G and $b(^{13}C) = 10 \pm 1$ G).

As shown above, sample heating to room temperature is accompanied by the transformation of radicals **A**

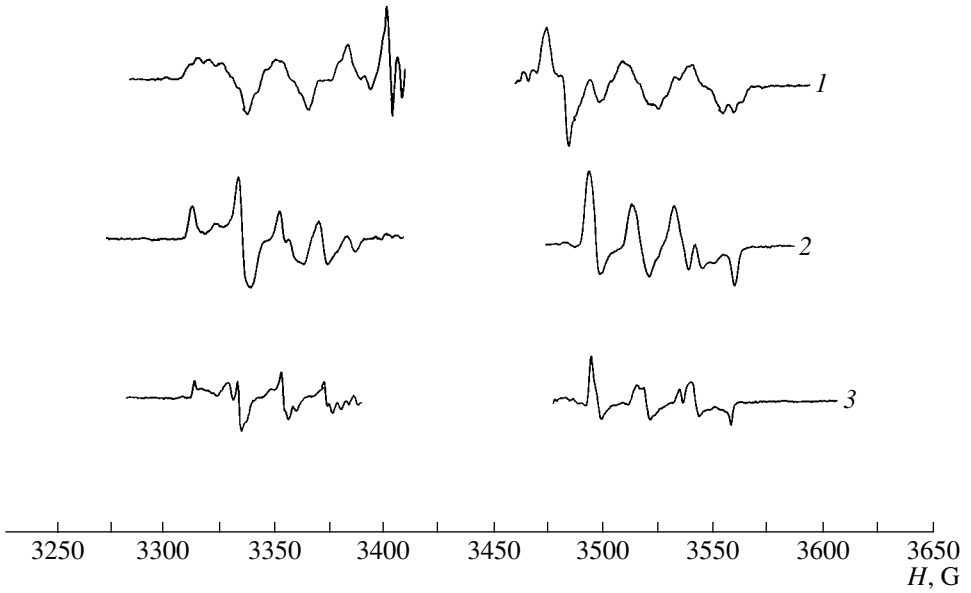

Fig. 8. ESR spectra radicals ≡Si–ND–^{13}C˙=O: (*1*) the product of ≡Si–˙N–D interaction with CO at 77 K (radical A); (*2*, *3*) after heating the product characterized by spectrum *1* to 300 K (radical **B**); the spectra were registered at (*2*) 77 and (*3*) 300 K.

into radicals **B**. The ESR spectra of radicals of this type containing ^{13}C are shown in Fig. 8 (curves *2* and *3*). The resolution of these spectra is much better than that of radicals **A**. This is due to the low value of the constant of HFI with the nucleus of deuterium (and proton in the hydrogen-containing center; see above) for these radicals. The tensor of HFI of an unpaired electron with the nucleus ^{13}C at 77 K in radical **B** is $a_{\|}(^{13}C) = (207 \pm 1)$ G and $a_{\perp}(^{13}C) = (159.5 \pm 1)$ G ($a_{iso}(^{13}C) = 175 \pm 2$ G and $b(^{13}C) = 16 \pm 1$ G). At 300 K: $a_{\|}(^{13}C) = (201.5 \pm 1)$ G and $a_{\perp}(^{13}C) = (166 \pm 1)$ G ($a_{iso}(^{13}C) = 178 \pm 2$ G and $b(^{13}C) = 12 \pm 1$ G). A change in the value *b* with temperature points to unfreezing of the internal motions in the radicals, which average the anisotropic components of the HFI tensor.

The isotropic and anisotropic components of the tensor of HFI of an unpaired electron with the nucleus ^{13}C determined experimentally for radicals **A** and **B** point to the fact that a considerable portion of the spin density is localized on the 2*s*- and 2*p* atomic orbitals of carbon in these radicals. This is a characteristic feature of acyl radicals X–C˙=O [23].

The relationship between the radiospectroscopic characteristics of radicals observed and their geometries was found using quantum chemical calculation [26]. Radicals $F_2(HO)Si–HN–C^{\bullet}=O$ and $F_3Si–HN–C^{\bullet}=O$ were used as models of active surface centers. Several local minimums were found on the potential energy surface of the radical $F_2(HO)Si–HN–C^{\bullet}=O$; these correspond to different orientations of the fragments SiNCO and HOSiN. The structure with spatial symmetry C_s (Fig. 9a) has the lowest energy. In this structure, atoms O, C, N, and Si are in the *cis*-configuration, and then the hydrogen atom of the hydroxyl group and the oxygen atom of the O=C groups are close to each other ($\angle$HOSiN = 0° and $R(H\cdots O) = 0.207$ nm); that is, they form an intramolecular hydrogen bond. The heat of formation of this conformer is 1.5 kcal/mol lower than the most stable of the *trans*-structure. For the *trans*-configuration of the SiNCO fragment on the potential energy surface, several local minimums corresponding to various arrangements of substituents at the silicon atom: the OH group and the NCO fragment. Two configurations of this sort, which differ in their energies by 0.1 kcal/mol, are shown in Figs. 9b and 9c.

For the radical $F_3Si–HN–C^{\bullet}=O$ (Figs. 9d, 9e), two minimums on the potential energy surface correspond to the *cis*- and *trans*-configurations of atoms O, C, N, and Si (symmetry C_s; $\angle$OCNSi = 0° or 180°, respectively). The energy of the latter configuration is 0.3 kcal/mol lower. Thus, the replacement of F at the silicon atom by the hydroxyl group leads to the stabilization of the *cis*-conformation of the radical. This is probably associated with the possibility of formation of the intramolecular hydrogen bond in this case.

The ground electronic state of *cis*- and *trans*-configurations of radicals with spatial symmetry C_s is $^2A'$. In this state, the main portion of spin density (~80%) is localized on the hybrid atomic orbital of carbon whose symmetry axis is in the plane of atoms N, C, and O and at an angle of ~122° to the axis of the C=O bond.

Table 2 shows the values of the HFI constants calculated for various conformations of the radicals $F_2(HO)Si–HN–C^{\bullet}=O$ (nos. 1–3) and $F_3Si–HN–C^{\bullet}=O$

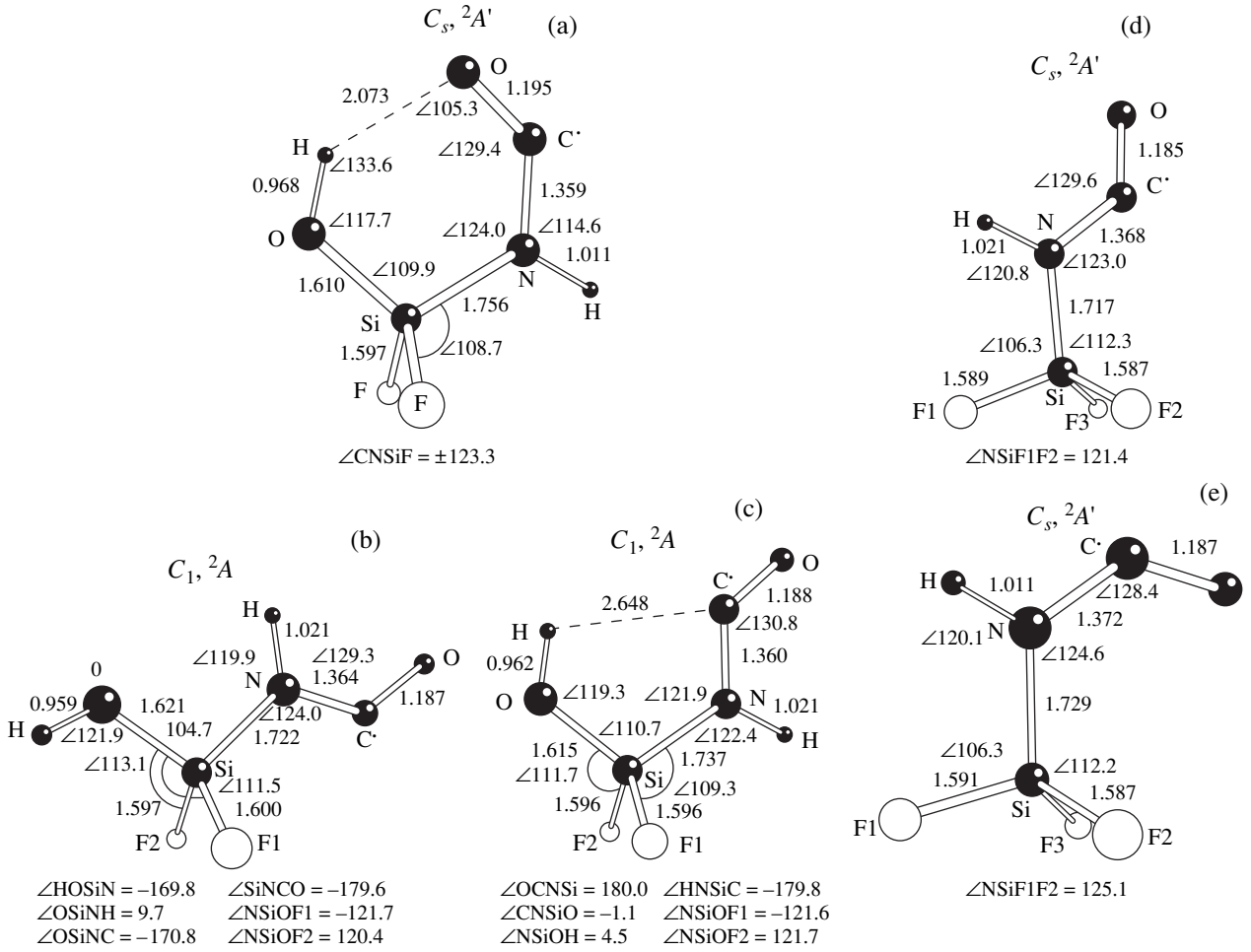

Fig. 9. Optimized structures of spatial isomers of radicals (a, b, c) $F_2(HO)Si–NH–\dot{C}=O$ and (d, e) $F_3Si–NH–\dot{C}=O$ (DFT calculation, UB3LYP/(6–311(*d*, *p*)). Bond lengths are in Å; angles are in degrees.

(nos. 4, 5), whose structures are shown in Figs. 9a–9d, respectively. According to the results of calculation, the *cis*- and *trans*-conformations of radicals ≡Si–HN–$\dot{C}$=O gave substantially different constants of HFI of an unpaired electron with substituents H and Si at the nitrogen atom. For the *cis*-configuration of radicals (nos. 1, 5 in Table 2), $a_{iso}(H(NH)) \ll a_{iso}(^{29}Si)$. For the *trans*-configuration (nos. 2–4 in Table 2), the situation is reversed. The values of HFI constants for these two conformations are close to the experimentally determined values for radicals **A** and **B**, respectively. Thus, the addition of a CO molecule to the radical ≡Si–$\dot{N}$–H at low temperatures leads to the formation of the radical ≡Si–HN–$\dot{C}$=O in the *trans*-configuration. This configuration is stable at temperatures lower than 160 K. On heating, it transforms into the more stable *cis*-conformation. This process is registered by the ESR method as the transformation of radical **A** into **B**. As mentioned above, there is equilibrium between these two radical forms *cis*-(≡Si–HN–$\dot{C}$=O) $\rightleftarrows$ *trans*-(≡Si–HN–$\dot{C}$=O). The equilibrium constant at 300 K is 0.25 ± 0.1. If we relate the effect observed to the difference in the heats of formation of the radicals, then we find that the *cis*-conformation is more stable than the *trans*-conformation by ~1 kcal/mol. This value agrees with the result of calculation: the *cis*-conformation of the radical $F_2(HO)Si–HN–\dot{C}=O$, which is the low-molecular model of the surface center $(≡Si–O)_2(HO)Si–HN–\dot{C}=O$, has an energy that is 1.5 kcal/mol lower than the *trans*-conformation.

3.1. Kinetics of *trans–cis* transformation of the ≡Si–HN–$\dot{C}$=O. Figure 10a shows the structure of the transition state for the reaction of CO addition to the radical $F_3Si–\dot{N}–H$ (DFT//B3LYP/6–311G(*d*, *p*) calculation). The activation energy of this reaction is as low as 0.2 kcal/mol. The calculation of the trajectory of CO motion from the transition state showed that the radical $F_3Si–HN–\dot{C}=O$ is preferably formed in the *trans*-conformation. This agrees with experimental data, according to which the addition of CO to the amino radical

Table 2. Calculated HFI constants for (1, 5) *cis*- and (2, 3, 4) *trans*-conformations of the Si–N–C–O group in the radicals (1, 2, 3) F_2(HO)Si–HN–C•=O and (4, 5) F_3Si–HN–C•=O (4, 5)*

No.	^{13}C	^{14}N	^{1}H(N)	^{29}Si	^{1}H(O)
1	175.8	20.7	3.3	–31.6	–0.8
	(–17.3, –15.2, 32.5)	(–2.1, –1.4, 3.5)	(–4.0, –2.6, 6.6)	(1.5, 1.3, –2.8)	(–2.3, –0.7, 3.0)
2	147.2	30.3	25.5	2.7	–0.9
	(–15.4, –14.2, 29.6)	(–1.7, –1.3, 2.9)	(–2.7, –0.7, 3.4)	(0.3, 0.3, –0.6)	(–2.4, –1.0, 3.4)
3	162.5	32.5	28.1	3.1	–0.1
	(–16.2, –14.7, 31.0)	(–1.6, –1.3, 2.9)	(–2.7, –0.8, 3.5)	(0.2, 0.2, –0.4)	(–0.5, –0.4, 0.9)
4	163.6	33.4	28.1	3.7	–
	(–16.1, –14.6, 30.7)	(–1.6, –1.3, 2.9)	(–2.7, –0.8, 3.5)	(0.3, 0.2, –0.5)	–
5	173.7	25.9	0.4	–35.8	–
	(–16.6, –14.7, 31.3)	(–1.9, –1.4, 3.3)	(–3.9, –2.5, 6.4)	(1.6, 1.4, –3.0)	–

Note: DFT calculation (UB3LYP/6–311G(*d*, *p*); the constants are in G. The first row shows the values of isotropic components. The next row (in parentheses) shows the principal values of the tensor of anisotropic HFI of an unpaired electron with the corresponding nucleus.

* Optimized structures of these radicals are shown in Fig. 9 (structures a–e, respectively).

occurs at a temperature as low as 77 K; that is, the activation energy of this reaction is low and the reaction leads to the formation of the radical in the *trans*-conformation.

Sample treatment at 158 K for 5 min did not result in noticeable changes in the form of the ESR spectrum of radicals **A**, whereas the transition was almost fully completed in 5 min at 190 K. This means that the rate constant $k(T) = k_0\exp(-E/RT)$ of the *trans–cis* isomerization of the acyl radical is lower than 2×10^{-4} s^{-1} at 160 K (T_1) and higher than 1×10^{-2} s^{-1} at 190 K (T_2). Assuming that the preexponential factor for the rate constant of this unimolecular process is equal to 10^{13} s^{-1}, we obtain $\exp(-E/RT_1) < 2 \times 10^{-17}$ and $\exp(-E/RT_2) > 1 \times 10^{-15}$; that is, $13.1 > E > 12.3$ kcal/mol.

The isomerization of the *trans*-conformation of the acyl radical to the *cis*-conformation can occur by the rotation of the C=O group around the N–C bond or by the unbending of the valence angle O=C–N. Figures 10b and 10c show the structures of two transition states corresponding to these channels of the reaction for the radical F_3Si–HN–C•=O. The activation energy calculated for the radical rearrangement is 13.2 kcal/mol in the first case and 30.6 kcal/mol (much higher) in the second case. Thus, we should expect that the first channel of transformation is preferable because its calculated activation energy is in acceptable agreement with the above experimental estimate.

3.2. On the intramolecular mobility of radicals A and B. Information on the nature of intramolecular mobility in a radical can be obtained when the motions of atoms change the ESR spectrum by at least partial averaging of the anisotropic components of the *g*-tensor or the tensors of HFI of an unpaired electron with magnetic nuclei. This is possible when the frequencies of the corresponding motions (ν) meet the condition $\nu\Delta H \geq 1$, where ΔH is the amplitude of the value averaged due to the motion [23]. To estimate the frequencies of separate internal motions in the radical F_2(HO)Si–HN–C•=O using quantum chemical methods, the corresponding potential energy surface profiles were calculated.

For the rotation of the C=O group around the N–C bond, there is a maximum on the potential energy surface when the value of the dihedral angle between the atoms O, C, N, and H is ~90°. This maximum corresponds to the transition state for the *trans–cis* isomerization of the radical. The height of the barrier for this isomerization (E) is higher than 10 kcal/mol. This means that the frequency of *cis–trans* transitions in the radical is not higher than 10^6 s^{-1} ($10^{13}\exp(-E/RT)$) at 300 K and, therefore, they should be reflected in the form of the ESR spectrum. The internal motion of another type is the rotation of the fragment NH–C=O around the Si–N bond. The profiles of the potential energy surface for this rotation were calculated for the *trans*- and *cis*-conformations of the radical. In this calculation, we froze the value of the dihedral angle OCNSi and optimized the rest of the system geometry, including the orientation of the OH group (the value of the dihedral angle NSiOH). According to the calculation, the height of the barrier E to the rotation of the fragment OCNH in the *trans*-conformation of the radical should be at most 1 kcal/mol. Therefore, the frequency of rotation of this fragment at 77 K should be higher 10^{10} s^{-1} ($10^{13}\exp(-E/RT)$). This would lead to the corresponding averaging of the anisotropic components of the *g*-tensor and HFI tensors. The height of the barrier to the rotation of this fragment in the *cis*-conformation of the radical was found to be lower (rotation is accompanied by the cleavage of the intramolecular

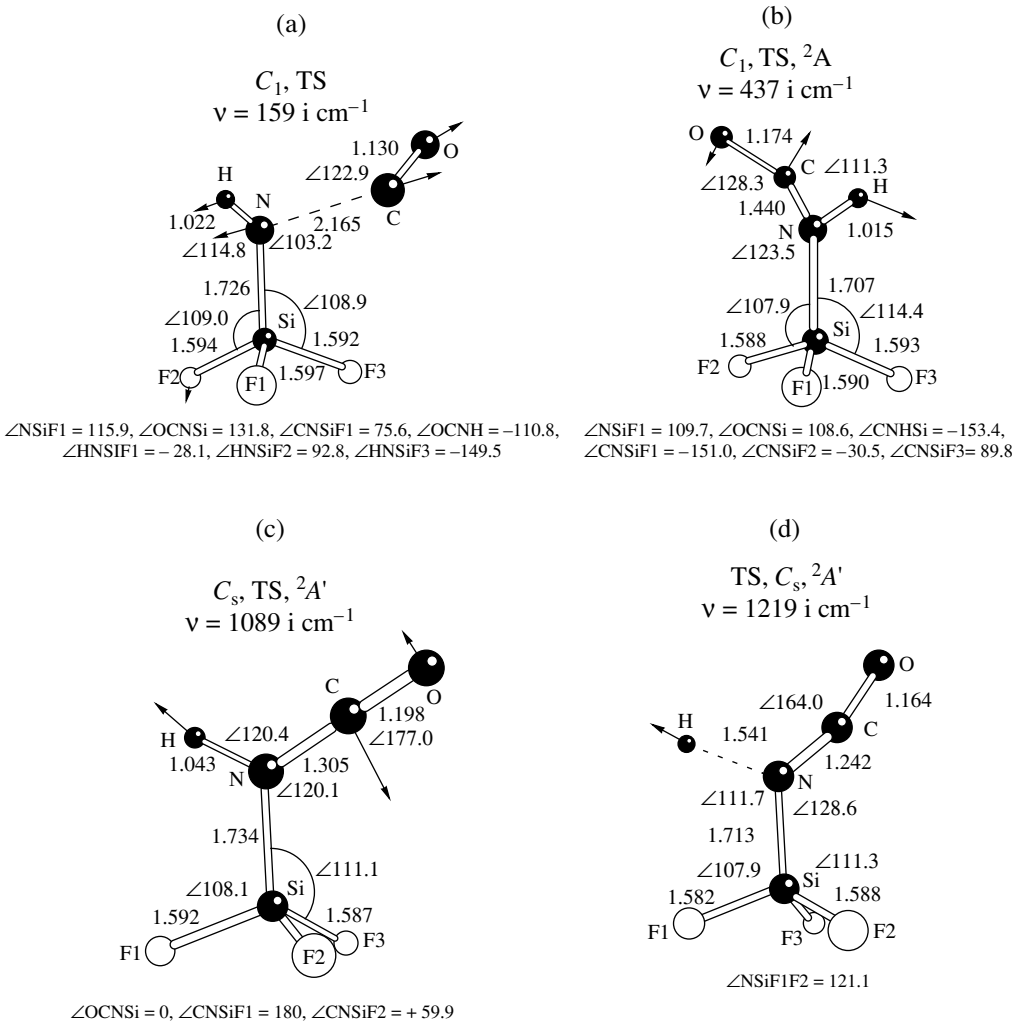

Fig. 10. Structures of transition states (TS) for the processes with the participation of the radicals $F_3Si–NH–\dot{C}=O$ (the imaginary frequency that characterizes the corresponding TS is given. The arrows show the shifts of atoms along the reaction coordinate. Calculations were performed by the density functional theory, UB3LYP/(6–311(*d, p*)). (a) Reaction $F_3Si–\dot{N}H + CO \rightleftharpoons F_3Si–NH–\dot{C}=O$; (b) *cis–trans* isomerization of $F_3Si–NH–\dot{C}=O$ as a result of the rotation of the CO group around the N–C bond; (c) reaction of *cis–trans* isomerization of the radical $F_3Si–NH–\dot{C}=O$ by opening of the NCO angle; and (d) reaction $F_3Si–NH–\dot{C}=O \longrightarrow F_3Si–N=C=O + H$. The bond lengths are in Å; the angles are in degrees.

hydrogen bond): ~4.5 kcal/mol. However, at 300 K the frequency of the corresponding motion is higher than 10^9 s^{-1} ($10^{13}\exp(-E/RT)$ s^{-1}).

Let us now turn to the experimental results. We expected that the *g*-tensors of radicals **A** and **B** have close principal values. They are determined (see formula (1)) by the position of the electronically excited states, which hardly changes in the transition from the *trans*- to *cis*-conformation of the radicals. Indeed, the isotropic value of the *g*-factors of radicals **A** (g_{iso} = 2.0018 ± 0.0002) and **B** (g_{iso} =2.0020 ± 0.0002) are close. However, the ESR spectrum of radical **B** at 300 K does not contain the same anisotropy of the *g*-tensor that was observed for the radical **A** at 77 K. In acyl radicals, the component of the *g*-tensor directed along the C=O bond (1.9983 for radical **A**) differs most greatly from the value characteristic of the free spin (2.0023) C=O [26]. In radical **A**, the angle between the direction of this bond and the Si–N bond (Fig. 9a) is ~5°. Therefore, even in the case of the monoaxial rotation of the radical around the Si–N bond, this rotation should not lead to the efficient averaging of the *g*-tensor anisotropy. The situation is different for radical **B**. For the *cis*-conformation of the fragment Si–N–C=O, the directions of the C=O bond and the Si–N bond are at an angle of 73.5°. Therefore, rotation or libration around the Si–N bond with a higher amplitude would result in the more efficient averaging of the *g*-tensor anisotropy.

Therefore, we can assume that the rotation in radical **B** around the Si–N bond is unfrozen at 300 K. The above results of quantum chemical calculation also provide evidence for that.

Among the HFI tensors for the acyl radicals (Table 2), high anisotropic components should largely be expected for the tensor of HFI of an unpaired electron with the nucleus ^{13}C. This tensor is close to axially symmetric, and the direction of the symmetry axis for the *trans*-conformation of the radical $F_3Si–HN–C^{\bullet}=O$ is at an angle of 59° to the Si–N bond. In the case of the *cis*-conformation, this angle is 9° (according to quantum chemical calculation, the directions of the symmetry axis and the bisector of the N–C=O angle only differ by 7°). This means that for the *cis*-conformation (radical **B**) the monoaxial rotation around the Si–N bond should not lead to a noticeable averaging of the anisotropic components of the corresponding tensor. Therefore, the anisotropy value experimentally observed at 300 K for radical **B**, which is close to the values expected for the unfrozen radical (Table 2), does not conflict with the conclusion based on the analysis of the value of the *g*-factor that the rotation around the Si–N bond is unfrozen at 300 K in this radical.

3.3. Thermal stability of the radicals ≡Si–HN–C•=O. The radicals ≡Si–HN–C•=O are stable at room temperature, but with an increase in temperature they decay. The process was monitored by the ESR method. A decrease in the concentration of radicals is accompanied by the appearance of two new paramagnetic centers. The ESR spectrum of one of them is a characteristic doublet with a splitting of ~80 G. This doublet belongs to the radical $>Si^{\bullet}–H$ [27]. Radicals of this sort are formed by the addition of hydrogen atoms to the diamagnetic silylene centers (reaction (VI)), which are present on the surface of reactive silica (see section 1) and are efficient hydrogen atom acceptors [1, 2]. Thus, one of the channels for the thermal transformation of the radicals ≡Si–HN–C•=O is their decay with the elimination of hydrogen atoms. Another radical product of the transformation is the radical ≡Si–N•–H. Its formation points to the fact that the thermal decomposition of the radical with the elimination of the CO molecule occurs at a comparable rate. Thus, the thermal decomposition of radicals ≡Si–HN–C•=O occurs via two channels:

$$\equiv Si–HN–C^{\bullet}=O \longrightarrow \equiv Si–N=C=O + H, \qquad (VII)$$

$$\equiv Si–HN–C^{\bullet}=O \longrightarrow \equiv Si–N^{\bullet}–H + CO. \qquad (VIII)$$

The overall rate constant of radical ≡Si–HN–C•=O decay was determined from data on the changes of intensities of their ESR signal when the sample was heated. The concentration of radicals decreased by a factor of 1.6 for 60 min at 373 K (k (373 K)= $(2.5 \pm 0.2) \times 10^{-4}$ s^{-1}). Heating at 402 K for 15 min led to a decrease in the concentration of radicals by a factor of 1.6 (k (402 K) = $(5.1 \pm 0.4) \times 10^{-4}$ s^{-1}). For 15 min at 415 K, the concentration of radicals decreased 2.4 times (k (415 K)= $(1.0 \pm 0.1) \times 10^{-3}$ s^{-1}). These experimental data suggest that the activation energy of the process is 29.5 ± 1 kcal/mol, assuming the standard preexponential factor (10^{13} s^{-1}).

The addition of the CO molecule to the radical ≡Si–N•H has an activation energy that is probably lower than 2 kcal/mol (the reaction occurs at low CO pressures and 77 K). Then, the estimated enthalpy of reaction (VIII) is 27–30 kcal/mol.

Below we provide the calculated activation energies and enthalpies of various channels of unimolecular $F_3Si–NH–C^{\bullet}=O$ decay. This radical is a model of the surface center. Calculation of the transition state structures and initial and final species and the energetics of these processes with the participation of this radical were carried out at the DFT level. Analogous calculations were carried out for the radical $H–NH–C^{\bullet}=O$ and supplemented with energy calculation of the corresponding structures at the G2MP2//UB3LYP level (shown in the scheme in parentheses; all energies are in kcal/mol).[3]

$$H_2N–C^{\bullet}=O \longrightarrow \mathbf{TS} + 26.2(23.9) \longrightarrow H_2N^{\bullet} + C=O + 24.7(20.6), \qquad (IX)$$

$$H_2N–C^{\bullet}=O \longrightarrow \mathbf{TS} + 31.6(34.8) \longrightarrow H + HN=C=O + 26.9(24.4), \qquad (X)$$

$$F_3Si–NH–C^{\bullet}=O \longrightarrow \mathbf{TS} + 27.0 \longrightarrow F_3Si–N^{\bullet}H + C=O + 26.8, \qquad (XI)$$

$$F_3Si–NH–C^{\bullet}=O \longrightarrow \mathbf{TS} + 27.8 \longrightarrow F_3Si–N=C=O + H + 16.4. \qquad (XII)$$

Let us first discuss the results of calculations for the radical $H_2N–C^{\bullet}=O$. According to experimental data, the activation energy of reaction (IX) is 25 kcal/mol [28]. Calculations give a close value. When estimating the enthalpy of reaction (IX), Yokota and Back [28] assumed that the activation energy of CO addition is ~5 kcal/mol (as for the reaction $H_3C^{\bullet} + CO \longrightarrow H_3C–C^{\bullet}=O$ [29]). According to our calculations at the same theoretical level (DFT//UB3LYP/6–311G**), the activation energy of the latter reaction is almost 3 kcal/mol higher. This indicates that the assumption that the activation energies of CO addition to the methyl

[3] The results of the calculation of enthalpies of these and other reactions at the G2MP2//B3LYP level are collected in Table 3.

Table 3. Thermochemical characteristics (ΔH(0 K)) for the processes with the participation of isoelectronic radicals $F_3Si{-}N^{\bullet}{-}H$ and $F_3Si{-}O^{\bullet}$ calculated at the G2MP2 level (values calculated by DFT calculations or obtained in experiments are given in parentheses (ΔH(298 K) [32])

Reaction	ΔH(0 K), kcal/mol
$F_3Si{-}N^{\bullet}{-}H \longrightarrow F_3Si^{\bullet} + NH(^3\Sigma_g)$	96.6 (91.2)
$F_3Si{-}N^{\bullet}{-}H \longrightarrow F_3SiN(^3A_1) + H$	99.6 (97.7)
$F_3Si{-}O^{\bullet} \longrightarrow F_3Si^{\bullet} + O(^3P)$	114.8 (108.6)
$F_3Si{-}N^{\bullet}{-}H + H_2 \longrightarrow F_3Si{-}NH_2 + H$	–11.8 (–8.3)
$F_3Si{-}O^{\bullet} + H_2 \longrightarrow F_3Si{-}OH + H$	–23.1 (–16.7)
$F_3Si{-}NH_2 \longrightarrow F_3Si{-}N^{\bullet}{-}H + H$	116.2 (112.0)
$F_3Si{-}OH \longrightarrow F_3Si{-}O^{\bullet} + H$	127.4 (120.3)
$F_3Si{-}NH_2 \longrightarrow F_3Si^{\bullet} + H_2N^{\bullet}$	120.5 (112.6)
$F_3Si{-}OH \longrightarrow F_3Si^{\bullet} + HO^{\bullet}$	140.4 (129.4)
$F_3Si{-}N^{\bullet}{-}H + CO \longrightarrow F_3Si^{\bullet} + HNCO$	10.5 (2.9)
$F_3Si{-}O^{\bullet} + CO \longrightarrow F_3Si^{\bullet} + OCO$	–12.3 (–18.7)
$F_3Si{-}N{=}C{=}O \longrightarrow F_3Si{-}N(^3A_1) + CO$	107.7 (–18.7)
$F_3Si{-}N{=}C{=}O \longrightarrow F_3Si^{\bullet} + {}^{\bullet}N{=}C{=}O$	131.7 (–18.7)
$H{-}N{=}C{=}O \longrightarrow HN(^3\Sigma_g) + C{=}O$	86.1 (exptl 88.6)
$H{-}N{=}C{=}O \longrightarrow H + {}^{\bullet}N{=}C{=}O$	113.1 (exptl 114.1)
$O{=}C{=}O \longrightarrow O(^3P) + C{=}O$	127.1 (exptl 127.2)
$H_2N{-}H \longrightarrow H_2N^{\bullet} + H$	106.7 (exptl 108.2)
$HN^{\bullet}{-}H \longrightarrow HN + H$	92.3 (exptl 97.0)
$HN(^3\Sigma_g) \longrightarrow N(^4S) + H$	77.6 (exptl 75.1)
$H_2N{-}C^{\bullet}{=}O \longrightarrow H + HN{=}C{=}O$	24.4
$H_2N{-}C^{\bullet}{=}O \longrightarrow H_2N^{\bullet} + C{=}O$	20.6
$HO{-}H \longrightarrow HO^{\bullet} + H$	118.7 (exptl 119.2)
$HO^{\bullet} \longrightarrow H + O(^3P)$	101.8 (exptl 102.4)

and nitrogen-centered radicals is barely correct. For the nitrogen-centered radical, the activation energy is lower than 3 kcal/mol. Thus, the results of calculations are in acceptable agreement with the experimental data for this radical and show that the two reactions of thermal decomposition considered above may occur at comparable rates in the values of enthalpies of reactions (XII) and (XIII).

The structure of the transition state for the radical $F_3Si{-}HN{-}C^{\bullet}{=}O$ decomposition with CO elimination is shown in Fig. 10a. Figure 10d shows the structure of the transition state for hydrogen atom elimination. The activation energies calculated by the DFT method for these channels of radical transformation are close and agree with the experimental estimate 29.5 ± 1 kcal/mol. To remind, the activation energy of CO addition to the radical $F_3Si{-}N^{\bullet}H$ is at most 1 kcal/mol.

In the calculations at the DFT level, the differences in the enthalpies of reactions (XI) and (XII) was found to be 10.4 kcal/mol. In the calculations at the G2MP2 level, this value was found to be 8.1 kcal/mol (see Table 3). Thus, the enthalpy of hydrogen atom abstraction from the radical $\equiv Si{-}HN{-}C^{\bullet}{=}O$ is ~22 kcal/mol.

The activation energy of another possible unimolecular decomposition of the radical $\equiv Si{-}HN{-}C^{\bullet}{=}O$

$$\equiv Si{-}HN{-}C^{\bullet}{=}O \longrightarrow \equiv Si^{\bullet} + HN{=}C{=}O \qquad \text{(XIII)}$$

is noticeably higher than for reactions (XI) and (XII). This conclusion is based on the quantum chemical calculation of the model reaction

$$F_3Si{-}NH{-}C^{\bullet}{=}O \longrightarrow \mathbf{TS} \longrightarrow F_3Si^{\bullet} + HN{=}C{=}O + 29.7. \qquad \text{(XIV)}$$

The difference in the enthalpies of reactions (XII) and (XIII) is 10.5 kcal/mol according to G2MP2 calculations (see Table 3). On the other hand, the activation energy of CO addition to the radical $F_3Si{-}N^{\bullet}H$ is close to zero (see above). Therefore, even if the activation energy of HN=C=O addition to the radical $F_3Si^{\bullet}$ is also close to zero, the activation energy of reaction (XIII) should be almost 10 kcal/mol higher than that of reaction (XII). This agrees with the observation that the products of the thermal decomposition of radicals $\equiv Si{-}HN{-}C^{\bullet}{=}O$ does not contain the radicals $\equiv Si^{\bullet}$.

4. Reaction $\equiv Si{-}N^{\bullet}{-}H + H_2 \longrightarrow \equiv Si{-}NH_2 + H$

When the radicals $\equiv Si{-}N^{\bullet}{-}H$ were treated in an H_2 atmosphere at room temperature, this gas is chemisorbed in the amount comparable with the number of radicals and the ESR spectrum of these radicals disappears (this spectrum is hard to register at 300 K, and we did it at 77 K). When the sample surface contained both the paramagnetic centers $\equiv Si{-}N^{\bullet}{-}H$ and the diamagnetic centers of silylene type ($(\equiv Si{-}O)_2Si$:), the decay of radicals in an atmosphere of H_2 was accompanied by the quantitative formation of new paramagnetic centers, radicals $\equiv Si^{\bullet}{-}H$. The appearance of the radicals

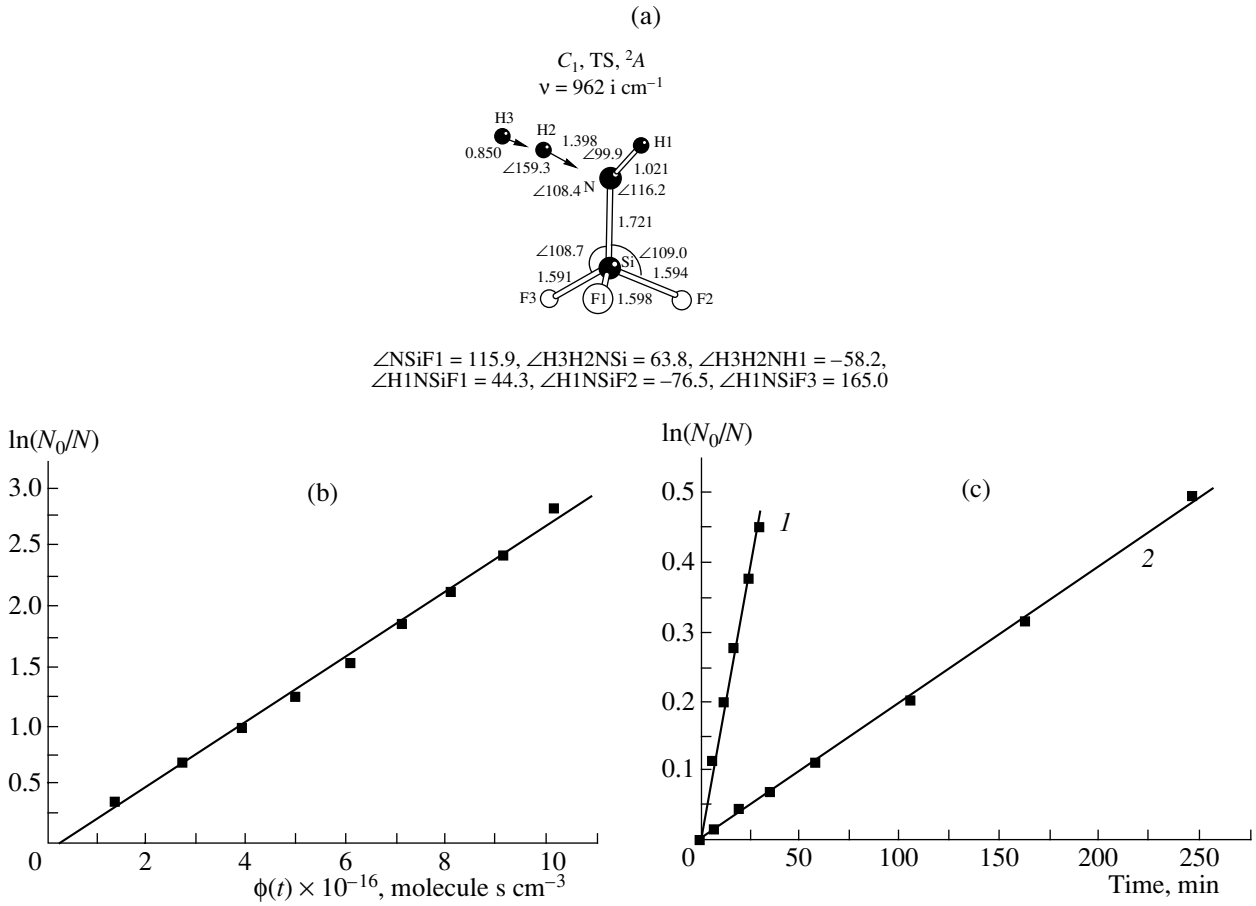

Fig. 11. Reaction of the radicals ≡Si–•N H with molecular hydrogen: (a) the structure of the transition state for the reaction F_3Si-•N H + H_2 ⟶ F_3Si–NH_2 + H (the imaginary frequency characterizing this TS is given and the arrows show the shifts of atoms as the system moves along the reaction coordinate; (b) kinetics of the radical ($(\equiv Si–O)_2(HO)Si–$•N H decay in the course of the reaction $(\equiv Si–O)_2(HO)Si–$•N H + H_2 ⟶ $(\equiv Si–O)_2(HO)Si–NH_2$ + H at 301 K in coordinates of Eq. (2); (c) kinetics of radical $(\equiv Si–O)_2(HO)Si–$•N H decay in the course of the reaction (*1*) $(\equiv Si–O)_2(HO)Si–$•N H + D_2 ⟶ $(\equiv Si–O)_2(HO)Si–NHD$ + D at 301 K and (*2*) the reaction $(\equiv Si–O)_2(HO)Si–$•N H + H_2 ⟶ $(\equiv Si–O)_2(HO)Si–NH_2$+ H at 77 K in semilogarithmic coordinates.

≡Si•–H point to the fact that hydrogen atoms are formed in the course of the reaction of ≡Si–N•–H with H_2 molecules:

$$\equiv Si–N^{\bullet}–H + H_2(D_2) \longrightarrow \equiv Si–NH_2(HD) + H(D) \quad (XV)$$

Hydrogen atoms are consumed in reaction (VI) by silylene groups, which are efficient acceptors of free radicals [1, 2].

Figure 11b shows the kinetics of radical ≡Si–N•–H decay in this process. In the course of the reaction, the hydrogen pressure decreased in the system. The rate of the bimolecular reaction under these conditions is

$$dN/dt = kP_{H_2}(t)N \text{ и } \ln(N_0/N) = k\int P_{H_2}(t)dt, \quad (2)$$

where k is the rate constant; N_0 and N are the initial and current concentrations of the radicals ≡Si–N•–H; $P_{H_2}(t)$ is the hydrogen pressure at the instant t; and $\int P_{H_2}(t)dt = \phi(t)$ is the exposure, which is a value proportional to the number of gas molecule collisions with the surface center for a period of time t. The straight line in Fig. 11b acceptably describes the linear law that follows from this equation. The rate constant determined from the slope of this straight line is k (301 K) = $(2.7 \pm 0.3) \times 10^{-17}$ cm^3 molecule^{-1} s^{-1}.

The reaction of radicals ≡Si–N•–H with deuterium molecules occurs in an analogous way (see the above scheme). The process was carried out at a concentration of D_2 in the gas phase of 2.2×10^{14} molecule/cm^3. The decay of nitrogen-centered radicals is accompanied by

the quantitative formation of deuterium atoms, which are accepted by the silylene centers with the formation of radicals $(\equiv Si–O)_2Si^{\bullet}–D$. These radicals were registered by the ESR method, and their characteristic spectrum is a triplet with an approximately 11 G splitting, which is due to the interaction of an unpaired electron with the deuterium nucleus. The kinetic curve of radical $\equiv Si–N^{\bullet}–H$ decay in this process is shown in Fig. 11c (curve *1*). The rate constant of the reaction of radicals $\equiv Si–N^{\bullet}–H$ with deuterium is $k(301\ K) = (5.1 \pm 0.5) \times 10^{-18}$ cm^3 molecule^{-1} s^{-1}. Thus, the value of the isotope effect for this reaction at room temperature is close to 5.

For reactions with the participation of hydrogen atoms, both the classical overcoming of the activation barrier and tunneling are possible. The value of the isotope effect points to the fact that at room temperature the reaction occurs via the classical over-the-barrier pathway. Assuming that the preexponential factor is 10^{-11} cm^3 molecule^{-1} s^{-1}, the activation energy of this reaction is $E = 7.7(8.7)$ kcal/mol for the processes with the participation of H_2 (D_2) molecules.

The rate constant of the reaction of the radical $\equiv Si–N^{\bullet}–H$ with the H_2 molecule extrapolated to 77 K (assuming the above activation energy) is 10^{-32} cm^3 molecule^{-1} s^{-1}. Therefore, at this temperature the reacting molecules cannot overcome the activation barrier via the classical pathway. However, the reaction of H_2 molecules with the radicals $\equiv Si–N^{\bullet}–H$ also occurs at 77 K. The process was carried out when the concentration of hydrogen molecules in the gas phase over the sample was 2.4×10^{15} molecule/cm^3. Note that hydrogen is practically not adsorbed on the silica surface under these conditions. As at 300 K, the decay of radicals $\equiv Si–N^{\bullet}–H$ is accompanied by the appearance of the radicals $>Si^{\bullet}–H$ in comparable amounts. These radicals are the products of hydrogen atom addition to the diamagnetic silylene centers (see reaction (VI)). Figure 11c (curve *2*) shows the kinetic curve for the decay of radicals $>Si–^{\bullet}NH$ in the course of the reaction at 77 K. A change in the hydrogen pressure of the sample by a factor of 5 led to a proportional increase in the reaction rate. Thus, the above experimental findings show that the reaction rate follows the rate law $-dN/dt = kNP_{H_2}$. The reaction rate constant determined from the slope of the straight line was $k(77\ K) = (1.35 \pm 0.1) \times 10^{-20}$ cm^3 molecule^{-1} s^{-1}.

The replacement of hydrogen by deuterium resulted in a drastic deceleration of the reaction. We did not find any trace of this reaction (with an accuracy of ±1%) when the sample was allowed to stay at 77 K and $P_{D_2} = 1 \times 10^{-1}$ Torr for 20 min. Therefore, the rate constant of the reaction with the participation of the D_2 molecule is at least 20 times lower.

The estimated reaction rate constant points to the fact that at 77 K the process occurs via the tunneling mechanism. In the simplest case of a tunneling reaction, where a species with the weight *m* tunnels through the parabolic barrier with a height *E* and the half-width *d*, the rate constant takes the following form [30]:

$$k = k_0\exp(-(2\pi^2/h)d(2mE)^{1/2}) = k_0\exp(-\gamma), \qquad (3)$$

where *h* is the Plank constant.

By comparing Eq. (3) with the measured rate constant of hydrogen atom abstraction at 77 K and assuming $k_0 = 10^{(-11 \pm 1)}$ cm^3 molecule^{-1} s^{-1} (which is a typical value for bimolecular reactions), we obtain $\gamma = 20 \pm 2$. Assuming that $E = 7.7$ kcal/mol, we obtain from Eq. (3) that the half-width of the activation barrier *d* is 0.05 ± 0.005 nm. According to the results of quantum chemical calculations (see Fig. 11), the distance between nitrogen and hydrogen atoms in the transition state of hydrogen atom transfer is ~0.14 nm, whereas the length of the N–H bond formed is ~0.10 nm. Assuming that the difference between these values (0.04 nm) characterizes the half-width of the potential barrier, we see that it is in acceptable agreement with the estimate based on experimental data.

A temperature at which the rates of over-the-barrier and tunneling pathways are equal is the so-called critical temperature [30]. If we assume that the rate constant measured at 77 K refers to the tunneling mechanism (and does not depend on temperature), whereas the rate constant measured at 300 K refers to the classical mechanisms (with overcoming a barrier of 7.7 kcal/mol), then the critical temperature of this reaction is ~190 K.

Figure 11a shows the structure of the transition state for the reaction of hydrogen atom abstraction from a hydrogen molecule by the radical $F_3Si–N^{\bullet}–H$, which is a low-molecular model of the surface center $\equiv Si–N^{\bullet}–H$. The scheme shows the results of calculation of the activation energy and the enthalpy of this reaction (the first value is the result of DFT calculation, and the second value is the result of calculation at the G2MP2 level (Table 3)). Analogous characteristics were also calculated for the reaction $H_2N^{\bullet} + H_2$ (for which literature data are available [31]):

$$F_3Si–N^{\bullet}–H + H_2 \longrightarrow \mathbf{TS} + 5.7\ (10.4)\ \text{kcal/mol}$$
$$\longrightarrow F_3Si–NH_2 + H - 8.3(-11.8)\ \text{kcal/mol},$$
$$H–N^{\bullet}–H + H_2 \longrightarrow \mathbf{TS} + 7.1\ (13.5)\ \text{kcal/mol}$$
$$\longrightarrow NH_3 + H + 1.1(-2.3)\ \text{kcal/mol}.$$

According to [31], the activation energy of the second reaction is ~9 kcal/mol, and its enthalpy (at 298 K) is –4 kcal/mol [32]. As expected, the calculation at the G2MP2 level provides better estimates of the reaction enthalpies. Overall, the results of calculation agree with

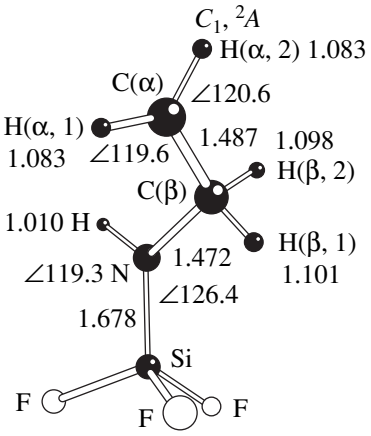

(a)

∠H(β, 1)C(β)C(α) = 107.2 ∠H(β, 2)C(β)C(α) = 111.0

∠SiNC(β)C(α) = –134.3 ∠H(α, 1)C(α)C(β)N = 37.5

∠H(α, 2)C(α)C(β)N = –152.1 ∠H(α, 1)C(α)C(β)H(α, 2) = –170.5

∠H(β, 2)C(β)C(α)H(α, 1) = 161.8 ∠H(β, 1)C(β)C(α)H(α, 1) = –81.9

∠HNC(β)C(α) = 53.4

>Si(OH)(NH–CH_2–$\dot{C}H_2$) (b)

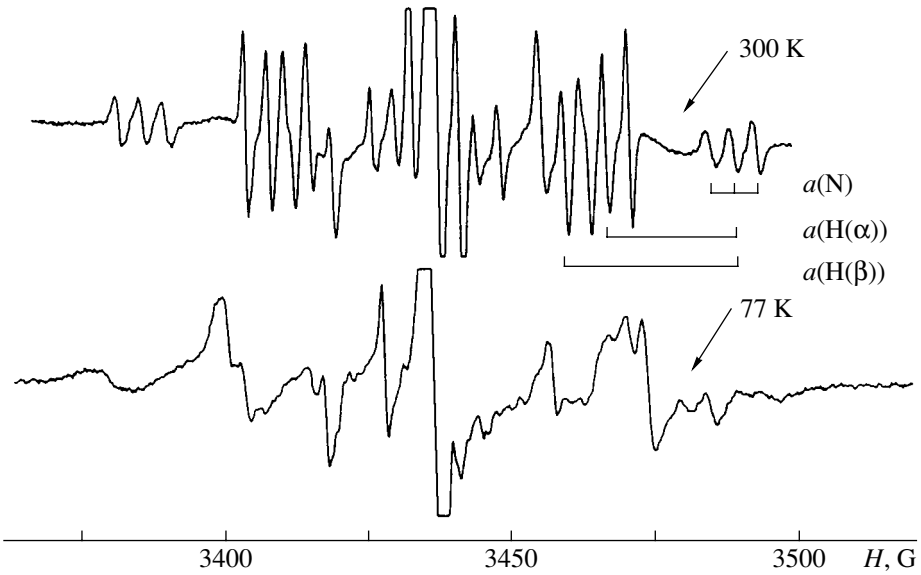

Fig. 12. The optimized structure of the radical (a) $F_3Si–HN–CH_2–\dot{C}H_2$ and the ESR spectrum of the radical (b) $(≡Si–O)_2(HO)Si–NH–CH_2–\dot{C}H_2$ (temperatures of registration 300 and 77 K).

experimental data and point to the fact that the reactivity of the silicon-containing radical $F_3Si–N^{\bullet}–H$ in this reaction is higher than the reactivity of $H–N^{\bullet}–H$. This is reflected in a decrease in the activation energy of the reaction and in an increase in its thermal effect.

Table 3 shows the results of calculating the thermal effects of some reactions with the participation of the radical $F_3Si–N^{\bullet}–H$ and the isoelectronic radical $F_3Si–O^{\bullet}$. G2MP2 calculations usually agree with experimental data within ±2 kcal/mol [12]. It fol-

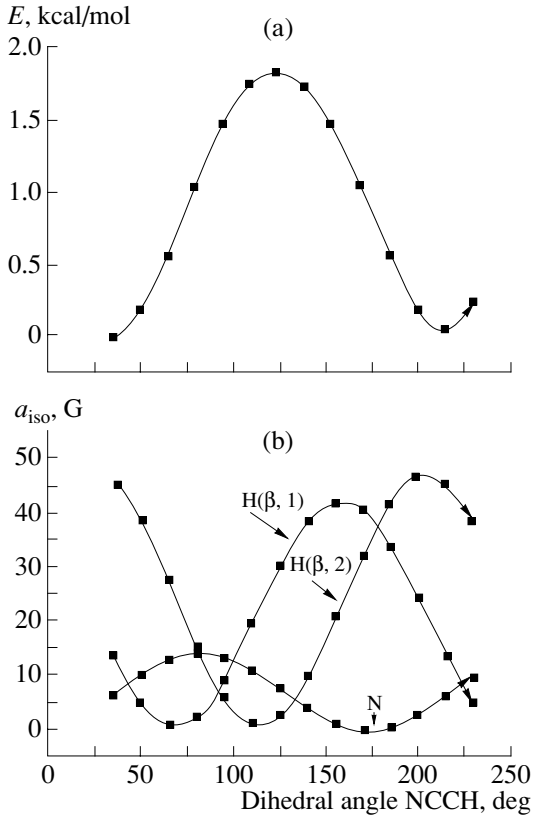

Fig. 13. The results of calculations of the dependence of (a) electronic energy and (b) the constants of isotropic HFI of an unpaired electron with β-protons and the nitrogen nucleus in the radical $F_3Si–HN–C(\beta)H_2–\dot{C}(\alpha)H_2$ on the angle of the internal rotation of the terminal CH_2 group around the C(α)–C(β) bond (DFT/UB3LYP/(6–311(*d, p*) calculation).

lows from the calculations presented that the strength of the Si–N bond in the molecules and radicals are 15–20 kcal/mol lower the corresponding Si–O bond, whereas the strength of the N–H bond is lower than the strength of the O–H bond by ~10 kcal/mol.

$$5.\ Reaction \equiv Si–\dot{N}–H + H_2C=CH_2 \longrightarrow \equiv Si–HN–\dot{C}(\beta)H_2–\dot{C}(\alpha)H_2$$

Figure 12b shows the ESR spectrum of the product of ethylene addition to the radical $\equiv Si–\dot{N}–H$. The reaction was carried out at 300 K and an ethylene pressure of 10^{-2} Torr. The hyperfine structure of the ESR spectrum is due to the interaction of an unpaired electron with two pairs of magnetically equivalent protons. The corresponding HFI constants are 22.3 ± 0.1 and 29.3 ± 0.2 G. Furthermore, each of the components splits into a triplet with the intensity ratios 1 : 1 : 1 and a distance between lines of 4.1 ± 0.1 G. Two pairs of magnetically equivalent protons are involved in the compositions of the groups $C(\alpha)H_2$ (22.3 G) and $C(\beta)H_2$ (29.3 G) of the radical. Close values of the constants of HFI with protons were registered for the radicals $\equiv Si–O–C(\beta)H_2–\dot{C}(\alpha)H_2$ (23.1 and 27.6 G, respectively) stabilized on the silica surface [3]. The triplet splitting is due to the interaction of an unpaired electron with the nitrogen nucleus, which is one of the substituents at the β-carbon atom in the radical. The HFI of an unpaired electron with the proton of the NH group of the radical in the form of the resolved hyperfine structure in the spectrum was not revealed ($a(H) \le 2$ G).

Figure 12a shows the optimized structure of the radical $F_3Si–HN–CH_2–\dot{C}H_2$, which is a model of the surface site. To check the applicability of the DFT method for determining the radiospectroscopic characteristics in radicals of this type, we calculated the constants of isotropic interaction of an unpaired electron with protons in the radical $H_3C(\beta)–\dot{C}(\alpha)H_2$. For the case of the free rotation of the methyl group, the values of $a_{iso}H(\beta)$ and $a_{iso}H(\alpha)$ were 27 and –22.85 G. The respective experimental values are 26.9 and –22.38 G [23]. For the equilibrium conformation of the radical $F_3Si–HN–CH_2–\dot{C}H_2$, the constants of isotropic HFI with protons of the $C(\alpha)H_2$ group are –21.2 G and those with the nitrogen nucleus are 5.5 G; protons of the group $C(\beta)H_2$ in the radical are magnetically nonequivalent. The constants of isotropic hyperfine splitting for them are 14.4 and 46.4 G. Figure 13 shows the results of calculation of the dependence of the electron energy of the radical and the constant of isotropic HFI of an unpaired electron with three substituents at the β-carbon atom (two protons and the ^{14}N nucleus) on the angle of the internal rotation of the terminal CH_2-group around the C(α)–C(β) bond. The height of the barrier for the internal rotation around the C(α)–C(β) bond is ~2 kcal/mol. A configuration obtained from that shown in Fig. 12a by mirror reflection of the terminal group $C(\alpha)H_2$ relative to the plane of atoms N, C(β), and C(α), has close energy, and the height of the activation barrier for this rotation is at most 2 kcal/mol (see Fig. 13a). At 300 K the frequency of such transitions is at least $10^{13}\exp(-E/RT) > 10^{11}$ s^{-1}. Under these conditions protons of the $C(\beta)H_2$ group are magnetically nonequivalent.

The constants of isotropic splitting on nitrogen nuclei and β-protons calculated for the model of free rotation around the C(α)–C(β) bond are $a_{iso}(N) = 7.0$ G and $a_{iso}H(\beta1) = a_{iso}H(\beta2) = 23$ G. Comparison of experimental constants obtained at 300 K and the results of calculations point to the fact that the value of splitting is lower on nitrogen and higher on the protons of the $C(\beta)H_2$ group than in the case of free rotation. Therefore, in the equilibrium conformation of the radical, the C(β)–N bond is inclined to the plane formed by the atoms of the terminal $C(\alpha)H_2$ group. This agrees with

the equilibrium geometry of this radical determined by quantum chemical calculations.

For the radicals of the considered type, the dependence of the constant of isotropic splitting with the nucleus of a substituent X at the β-carbon atom on the angle of the internal rotation around the C(α)–C(β) bond is usually described in the form $a_{iso}(X, \varphi) = A_0(X)\cos^2\varphi$, where φ is the dihedral angle between the axis of the 2*p* atomic orbital of the terminal carbon atom on which an unpaired electron is localized and the atoms C(α), C(β), and X. Using the results of calculation (see Fig. 13b) for the nitrogen atom in the radical $F_3Si–HN–CH_2–C^{\bullet}H_2$, we obtain $A_0(N) = 14$ G.

6. Reaction ≡Si–HN–C•=O + C_2H_4

The radicals ≡Si–HN–C•=O also react with ethylene molecules at room temperature. The reaction occurs even at low C_2H_4 pressures (10^{-3} Torr) and is accompanied by the disappearance of the ESR spectrum of radicals ≡Si–HN–C•=O and by the appearance of the new paramagnetic center in comparable amounts. The ESR spectrum of the radical formed is shown in Fig. 14. At 300 K, this spectrum is a triplet of triplets with the constants of hyperfine splitting of 22.8 ± 0.1 and 25.3 ± 0.1 G. At the edge components of the spectrum, additional poorly resolved hyperfine structure appears. It can be assigned to the interaction of an unpaired electron with the nitrogen nucleus in the radical. The value of this constant is 1.3 ± 0.1 G. Moreover, the constant of HFI of an unpaired electron with the ^{13}C nucleus for this radical was measured: $a_{iso}(^{13}C)$ = (14.7 ± 0.3) G. In this experiment we used CO enriched in the ^{13}C isotope in preparing the acyl radicals.

The spectrum has a form that is typical of hydrocarbon radicals X–C(β)H_2–Ċ(α)H_2. Earlier, radicals of this sort were synthesized on the silica surface as the products of the ethylene addition to other radicals stabilized on the SiO_2 surface: ≡Si•, ≡Si–O•, ≡Si–O–C•=O [1, 3]. Thus, the ESR signal belongs to the radicals ≡Si–HN–C(O)–C(β)H_2–Ċ(α)H_2. The constant of HFI equal to 22.8 G is due to the interaction of an unpaired electron with the protons of the C(α)H_2 groups, and that equal to 25.3 G is due to the interaction with protons of the C(β)H_2 group [3]. A change in the temperature of ESR spectrum registration (77 K) resulted in the reversible change in the form of the ESR spectrum (Fig. 14). This points to a change in the nature of rotational mobility in the radical around the bonds C–C(β) and C(β)–C(α) [3].

The synthesized hydrocarbon radicals react with H_2 at room temperature:

$$\equiv Si–HN–C(O)–C(\beta)H_2–\dot{C}(\alpha)H_2 + H_2$$

$$\equiv Si–NH–C(O)–C(\beta)H_2\dot{C}(\alpha)H_2$$

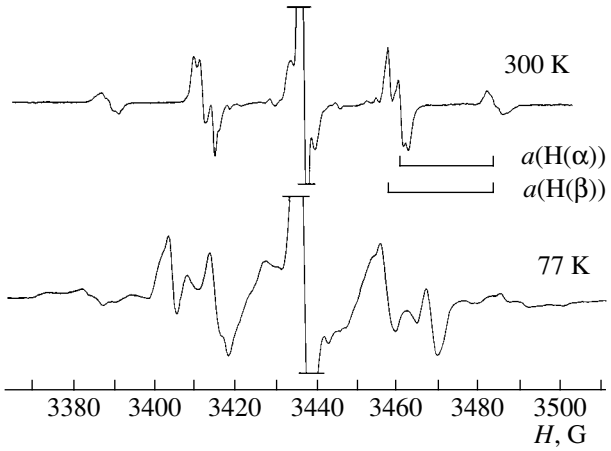

Fig. 14. ESR spectra of the products of C_2H_4 addition to the radical $(\equiv Si–O)_2(HO)Si–NH–\dot{C}=O$ (the registration temperatures are 300 and 77 K).

$$\longrightarrow \equiv Si–HN–C(O)–C(\beta)H_2–C(\alpha)H_3 + H,$$

whereas hydrogen atoms formed react with silylene centers by reaction (VI).

This is evidenced by the decay of hydrocarbon radicals and the appearance of the radicals >Si•–H in comparable amounts (see Section 4). The rate constant of this reaction was measured at 300 K (P_{H_2} = 2.7 ± 0.1 Torr): $k(300\ K) = (5.3 \pm 0.6) \times 10^{-21}$ cm^3 molecule^{-1} s^{-1}. According to [33], the rate constant of the analogous reaction with the participation of the radical ≡Si–O–C(β)H_2–C•(α)H_2 at room temperature is 2×10^{-20} cm^3 molecule^{-1} s^{-1}.

Thus, the fragment ≡Si–NH–C(O)–CH_2–R containing the amide group was assembled on the SiO_2 surface. The latter is a constituent of many compounds, including bioactive ones. The experimental data reported here demonstrate the possibility of molecular design on the reactive silica surface.

7. On the Expected Optical Characteristics of Radicals ≡Si–N•–H and ≡Si–HN–C•=O

Experimental data on the optical characteristics of these radicals have not been obtained. According to quantum chemical calculations, the relaxation of the first excited states of the radicals X–•N–Y is accompanied by a change in the geometry, which is basically reflected in an increase in the valence angle at the nitrogen atom. In the radicals H–•N–H, H–•N–F, and F–•N–F, this angle increases from 102.1°, 100.1°, and 103.6° to 144.9°, 121.9°, and 120.0°, respectively. The DFT-calculated vertical transitions to the excited state (absorption) and the reverse transition (in parentheses)

Table 4. Distribution of spin density in acyl radicals in the ground X($^2A'$) and first electronically excited A($^2A''$) states and the energies of vertical transitions (DFT/UB3LYP/6–31G(*d*, *p*) calculations)*

Radical structure	c_0^2 (O($2p_x$))	c_0^2 (C($2p_x$))	c_1^2 (O($2p_y$))	c_1^2 (C($2p_y$))	ΔE, eV (X ⟶ A)
H–C$^{\bullet}$=O (C_s)	0.27	0.31	0.26	0.73	2.22
F_3Si–HN–C$^{\bullet}$=O (C_s, ∠OCNSi = 180°)	0.28	0.30	0.20	0.69	3.81
F_2(HO)Si–HN–C$^{\bullet}$=O (C_s, ∠OCNSi = 0°, ∠HOSiN = 0°)	0.25	0.38	0.18	0.69	3.79
F_3Si–O–C$^{\bullet}$=O (C_s, ∠OCOSi = 180°)	0.28	0.30	0.20	0.69	3.83

* The coefficients c_0^2 and c_1^2 show the populations of atomic orbitals of oxygen and carbon atoms in the ground state ($^2A'$) and the first electronically excited state ($^2A''$) in acyl radicals. The *z* axis is directed along the C=O bond, and the *y* axis is perpendicular to the plane of atoms X–C=O (X=H, N, or O).

from the relaxed excited state to the ground state (luminescence) for these radicals are 2.14 (0.52); 2.70 (1.91); and 4.49 (3.74) eV. Based on the quantum chemical calculations (see Section 2.2), the radical ≡Si–N$^{\bullet}$–H has an absorption band in the near-infrared region (~1 eV). After vertical transition from the ground ($^2A''$) to the lower ($^2A'$) electronically excited state, the relaxation of its geometry is basically accompanied by a change in the value of the valence angle Si–N–H in the radical from 114.6° to ≈180°. As this takes place, the energies of states $^2A'$ and $^2A''$ become equal (degenerate state). After entering this region of the configurational space due to the converging and overlapping of electron terms, the system will return to the ground term but with strongly distorted geometry compared to the equilibrium one. As a result, the energy of electron excitation will transform into the energy of nucleus motion largely associated with the deformational vibration of the Si–N–H group (initial opening of the valence angle followed by the restoration of the equilibrium value). Thus, the radical F_3Si–$^{\bullet}$N–H in the state $^2A'$ can nonradiatively return to the ground state. In this case, the energy of electron excitation transforms into the energy of nucleus motion. As a result, we can assume that the absorption of a light quantum of ~1 eV by this radical should not be accompanied by luminescence. However, the energy of the electronically excited radical is insufficient for any chemical transformations (decomposition or isomerization). Similar optical properties are expectable for the radical ≡Si–N$^{\bullet}$–H stabilized on the silica surface.

The transition of acyl radicals X–C$^{\bullet}$=O from the ground state ($^2A'$) to the lower electronically excited state ($^2A''$) corresponds to the transfer of an unpaired electron to the π* molecular [34]. Table 4 shows the results of DFT calculations of spin densities in the ground state and the first excited state of the radical. The energies of these vertical transitions were found to be close for various structures and equal to ~3.8 eV. Experimental data on the position of the band of optical absorption of the radical ≡Si–HN–C$^{\bullet}$=O corresponding to these transitions have not yet been obtained, but such experimental data are available for the isoelectronic radical (≡Si–O)$_3$Si–O–C$^{\bullet}$=O stabilized on the silica surface [35]. For this radical, the band of optical absorption was registered with the maximum at 3.6 ± 0.1 eV. DFT calculation for the model low-molecular radical F_3Si–O–C$^{\bullet}$=O yielded a value of the vertical transition $^2A' \longrightarrow {}^2A''$ equal to 3.8 eV, which is the same as for radicals F_2(HO)Si–HN–C$^{\bullet}$=O and F_3Si–HN–C$^{\bullet}$=O. Based on the data presented, we may assume that the first band of optical absorption of the radical (≡Si–O)$_2$(HO)Si–HN–C$^{\bullet}$=O is near 3.6 eV ($\sigma \longrightarrow \pi^*$ transition).

According to calculation, the relaxation of the state $^2A''$ is accompanied by an increase in the valence angle N–C=O or O–C=O in the corresponding acyl radicals to ≅180°. As this takes place, the energies of the states $^2A''$ and $^2A'$ become comparable, and the electronic state becomes degenerate. Thus, as a result of relaxation of the radical geometry, it appears in the region of the configurational space, where two terms ($^2A''$ and $2A'$) become close and the transition between them becomes highly probable. This allows us to assume that the optical absorption at 3.6 eV may not be accompanied by luminescence. When the radical returns to the state $^2A'$, it is strongly deformed and vibrationally excited. Note that the energy of the electron excitation is sufficient for

radical decomposition. For instance, the activation energy of the thermal decomposition of the nitrogen-containing acyl radical with the elimination of the CO molecule is ~30 kcal/mol (1.3 eV) (Section 3.3). The channel for the phototransformation of the radical in the state $^2A''$ has not been determined. It was shown in [36] that the action of nonfiltered light of the high-pressure mercury lamp ($E \le 5.2$ eV) results in the photodecomposition of the radicals $(\equiv Si–O)_3Si–O–C^{\bullet}=O$ with the elimination of the CO molecule. However, it has not been established whether this reaction occurs from the lower electronically excited state.

ACKNOWLEDGMENTS

This work was supported by the Russian Foundation for Basic Research (project no. 00-03-32069). Calculations were carried out using GAUSSIAN-94 [8] within the framework of Russian Foundation for Basic Research grant no. 98-07-90290 at the Zelinskii Institute of Organic Chemistry, Russian Academy of Sciences.

REFERENCES

1. Radtsig, V.A., *Chem. Phys. Rep.*, 1995, vol. 14, no. 8, p. 1206.
2. Radtsig, V.A., *Kinet. Katal.*, 1999, vol. 40, no. 5, p. 764.
3. Radtsig, V.A., *Kinet. Katal.*, 1983, vol. 24, no. 1, p. 173.
4. Sarkisov, O.M. and Lozovskii, V.A., *Khim. Fiz.*, 1995, vol. 14, no. 9, p. 132.
5. Morterra, C. and Low, M.J.D., *J. Chem. Soc., Chem. Commun.*, 1968, no. 2, p. 203.
6. Morterra, C. and Low, M.J.D., *Ann. N. Y. Acad. Sci.*, 1972, vol. 220, no. 1, p. 135.
7. Radzig, V.A., *Colloids Surf. A*, 1993, vol. 74, no. 1, p. 91.
8. Frisch, M.J., Trucks, G.W., Schlegel, H.B., Gill, P.M.W., Johnson, B.G., Robb, M.A., Cheeseman, J.R., Keith, T., Petersson, G.A., Montgomery, J.A., Raghavachari, K., Al-Laham, M.A., Zakrzewski, V.G., Ortiz, J.V., Foresman, J.B., Cioslowski, J., Stefanov, B.B., Nanayakkara, A., Challacombe, M., Peng, C.Y., Ayala, P.Y., Chen, W., Wong, M.W., Andres, J.L., Replogle, E.S., Gomperts, R., Martin, R.L., Fox, D.J., Binkley, J.S., Defrees, D.J., Baker, J., Stewart, J.P., Head-Gordon, M., Gonzalez, C., and Pople, J.A., *Gaussian 94, Revision D. 1.*, Gaussian: Pittsburgh, 1995.
9. Radtsig, V.A., *Kinet. Katal.*, 1996, vol. 37, no. 2, p. 310.
10. Becke, A.D., *J. Chem. Phys.*, 1993, vol. 98, p. 5648.
11. Lee, C., Yang, W., and Parr, R.G., *Phys. Rev. B: Condens. Matter*, 1988, vol. 37, p. 785.
12. Curtiss, L.A., Raghavachari, K., and Pople, J.A., *J. Chem. Phys.*, 1993, vol. 98, no. 2, p. 1293.
13. Radtsig, V.A. and Kozlov, S.N., *Kinet. Katal.*, 2001, vol. 42, no. 1, p. 62.
14. Radtsig, V.A., *Kinet. Katal.*, 2001, vol. 42, no. 5, p. 696.
15. Bobyshev, A.A. and Radtsig, V.A., *Kinet. Katal.*, 1990, vol. 31, no. 4, p. 925.
16. Misochko, E.Ya., Goldschleger, I.U., and Akimov, A.V., *Fiz. Nizkikh Temp.* 2000, vol. 26, nos. 9/10, p. 981.
17. Kasai, P.H. and Whipple, E.B., *Mol. Phys.*, 1965, vol. 9, p. 497.
18. Mackey, J.H., Boss, J.W., and Kopp, M., *Phys. Chem. Glasses*, 1970, vol. 11, no. 6, p. 205.
19. Airey, W., Glidewell, C., Rankin, D.W.H., Robiette, A.G., Sheldrick, G.M., and Cruickshank, D.W.J., *Trans. Faraday Soc.*, 1970, vol. 66, p. 551.
20. Jacox, M.E., Milligan, D.E., Guillory, W.A., and Smith, J.J., *J. Mol. Spectrosc.*, 1974, vol. 52, p. 322.
21. Dressler, K. and Ramsay, D.A., *Phil. Trans. Roy. Soc.*, 1959, vol. A251, no. 1002, p. 553.
22. Kanzig, W. and Cohen, M.H., *Phys. Rev. Lett.*, 1959, vol. 3, p. 509.
23. Pshezhetskii, S.Ya., Kotov, A.G., Milinchuk, V.K., Roginskii, V.A., and Tupikov, V.I., *EPR svobodnykh radikalov v radiatsionnoi khimii* (EPR of Free Radicals in Radiation Chemistry), Moscow: Khimiya, 1972, p. 480.
24. Radtsig, V.A. and Bystrikov, A.V., *Kinet. Katal.*, 1978, vol. 19, p. 713.
25. Radtsig, V.A., *Khim. Fiz.*, 2002, vol. 21, no. 3, p. 52.
26. Barone, V., Adamo, C., and Russo, N., *Int. J. Quantum Chem.*, 1994, vol. 52, p. 963.
27. Radtsig, V.A., *Kinet. Katal.*, 1979, vol. 20, no. 2, p. 456.
28. Yokota, T. and Back, R.A., *Int. J. Chem. Kinet.*, 1973, vol. 5, no. 1, p. 37.
29. Watkins, K.W. and Word, W.W., *Int. J. Chem. Kinet.*, 1974, vol. 6, p. 855.
30. Gol'danskii, V.I., *Dokl. Akad. Nauk SSSR*, 1959, vol. 124, p. 1261.
31. Hack, W., Rouveirolles, P., and Wagner, H.G., *J. Phys. Chem.*, 1986, vol. 90, p. 2505.
32. Lias, S.G., Liebman, J.F., Levin, R.D., and Kafafi, S.A., *NIST Standart Reference Database 25. Structure and Properties*, 1994.
33. Bobyshev, A.A., Radtsig, V.A., and Senchenya, I.N., *Kinet. Katal.*, 1990, vol. 31, no. 4, p. 931.
34. Mel'nikov, M.Ya. and Smirnov, V.A., *Fotokhimiya organicheskikh radikalov* (Photochemistry of Organic Radicals), Moscow: Mosk. Gos. Univ., 1994.
35. Bobyshev, A.A. and Radtsig, V.A., *Fiz. Khim Stekla*, 1988, vol. 14, p. 501.
36. Bobyshev, A.A. and Radtsig, V.A., *Spektroskopiya stekloobrazuyushchikh sistem* (Spectroscopy of Glass-Forming Systems), Silin', A.R., Ed., Riga: Latv. Gos. Univ., 1988, p. 85.